Population-level asymmetry of the cerebral cortex: reproducibility, lifespan changes, heritability, and individual differences

Authors and affiliations

James M. Roe[1]*, Didac Vidal-Piñeiro[1], Inge K. Amlien[1], Mengyu Pan[1], Markus H. Sneve[1], Michel Thiebaut de Schotten[2,3], Patrick Friedrich[4], Zhiqiang Sha[5], Clyde Francks[5,6], Yunpeng Wang[1], Kristine B. Walhovd[1,7], Anders M. Fjell[1,7] & René Westerhausen[8]

[1]Center for Lifespan Changes in Brain and Cognition (LCBC), Department of Psychology, University of Oslo, Norway.
[2]Groupe d'Imagerie Neurofonctionnelle, Institut des Maladies Neurodégénératives-UMR 5293, CNRS, CEA, University of Bordeaux, Bordeaux, France.
[3]Brain Connectivity and Behaviour Laboratory, Sorbonne Universities, Paris, France.
[4]Institute of Neuroscience and Medicine (INM-7: Brain and Behaviour), Research Centre Jülich, Jülich, Germany.
[5]Language and Genetics Department, Max Planck Institute for Psycholinguistics, Nijmegen, The Netherlands.
[6]Donders Institute Netherlands for Brain, Cognition and Behaviour, Radboud University, Nijmegen, The Netherlands.
[7]Department of Radiology and Nuclear Medicine, Oslo University Hospital, Oslo, Norway.
[8]Section for Cognitive and Clinical Neuroscience, Department of Psychology, University of Oslo, Norway.

*Address correspondence to James M. Roe, Department of Psychology, PO Box 1094 Blindern, 0317 Oslo, Norway.
Email: j.m.roe@psykologi.uio.no

Running title: Population-level cortical asymmetry
Keywords: Lateralization, population neuroscience, lifespan
Open access license: yes

The authors declare no competing interests

Abstract

Cortical asymmetry is a ubiquitous feature of brain organization that is altered in neurodevelopmental disorders and aging. Achieving consensus on cortical asymmetries in humans is necessary to uncover the genetic-developmental mechanisms that shape them and factors moderating cortical lateralization. Here, we delineate population-level asymmetry in cortical thickness and surface area vertex-wise in 7 datasets and chart asymmetry trajectories across life (4-89 years; observations = 3937; 70% longitudinal). We reveal asymmetry interrelationships, heritability, and test associations in UK Biobank (N=~37,500). Cortical asymmetry was robust across datasets. Whereas areal asymmetry is predominantly stable across life, thickness asymmetry grows in development and declines in aging. Areal asymmetry correlates in specific regions, whereas thickness asymmetry is globally interrelated across cortex and suggests high directional variability in global thickness lateralization. Areal asymmetry is moderately heritable (max h^2_{SNP} ~19%), and phenotypic correlations are reflected by high genetic correlations, whereas heritability of thickness asymmetry is low. Finally, we detected an asymmetry association with cognition and confirm recently-reported handedness links. Results suggest areal asymmetry is developmentally stable and arises in early life, whereas developmental changes in thickness asymmetry may lead to directional variability of global thickness lateralization. Our results bear enough reproducibility to serve as a standard for future brain asymmetry studies.

Significance

Cortical asymmetry is reduced in neurodevelopmental disorders, yet we lack knowledge of how cortical asymmetry development proceeds across life in health. We provide a definitive reference for asymmetry in the cerebral cortex. We find areal asymmetry is stable from childhood to old age, and specific areal asymmetries are formed under common genetic-developmental influence. In contrast, thickness asymmetry shows developmental growth, and is globally interrelated in a pattern suggesting highly left-lateralized individuals tend towards left-lateralization also in right-asymmetric regions (and vice versa). Heritability mapping also supported a prenatal-postnatal developmental dichotomy for areal and thickness asymmetry, and we find reduced asymmetry in the most lateralized brain region associates with reduced cognition. Our results provide novel insights into normal brain organization and development.

1. Introduction

The brain's hemispheres exhibit high contralateral symmetry [1,2] and homotopic regions are amongst the most genetically [3–6] and developmentally linked [3,7]. However, structural asymmetry is also a ubiquitous aspect of brain organization [8,9]. For instance, cortical thickness (CT) and surface area (SA) are known to exhibit distinct asymmetry patterns [8,10], but these have been reported inconsistently [8,9,11–21]. Yet disrupted cortical asymmetry is a confirmed feature of neurodevelopmental disorders [22], aging [11], and Alzheimer's disease [11,23,24]. Hence, achieving consensus on cortical asymmetries and understanding the genetic-developmental and lifespan influences that shape and alter them is necessary to discover precise biomarkers for disease. To reach consensus, an atlas-free description of asymmetries that reliably replicate across international samples (i.e. population-level asymmetries) is needed. This would enable precision mapping of the genetic and individual-specific factors moderating cortical lateralization, and serve as a high-fidelity phenotype for future studies on brain asymmetry. Furthermore, it is unknown how cortical asymmetry development proceeds across life, as no previous study has mapped cortical asymmetry trajectories longitudinally across the lifespan.

Although several studies have mapped cortical asymmetry [8,9,11–21,25], conflicting results may be partly due to the use of brain atlases with varying resolutions of analysis, especially if cortical asymmetry conforms poorly to the predefined anatomical boundaries [26,27]. Still, even amongst studies adopting an atlas-free approach, conflicting results abound [14–19]. For example, for CT asymmetry, medial prefrontal cortex (mPFC) has been reported to show both extensive rightward [15,17,18] and leftward [11–13,21] lateralization. Beyond regional inconsistencies, a recent meta-analysis confirmed the cortex is globally organized in a characteristic pattern of CT asymmetry, wherein anterior and posterior regions are thicker in the left and right hemisphere, respectively [8]. Notably, while this agrees with some reports [12,13,21,28,29], it is less compatible with many others [9,14–20,30]. Furthermore, that study applied a relatively course brain atlas, and there is currently no high-resolution complement to describe cortical asymmetries that reliably reproduce across international samples (but see [11,29]). For areal asymmetry, while results have been broadly more consistent [8,9,15,20,25,31], there nevertheless remain important discrepancies, such as reports of right- [8,32,33] and left- [15,31] lateralization of superior temporal sulcus (STS).

An accurate description of the lifespan trajectories of cortical asymmetry may shed light on mechanisms underlying diverse aspects of asymmetry across life. For CT, longitudinal increases in asymmetry have been shown during the first two years of life [12], with suggestions of rapid asymmetry growth from birth to 1 year [12], and continued growth until adolescence [34]. However, previous studies mapped CT asymmetry linearly across cross-sectional developmental and adult age-ranges [14,21], mostly concluding CT asymmetry is minimal in infancy and maximal around age 60. In contrast, recent work established CT asymmetry shows a non-linear decline from 20 to 90 years that is reproducible across longitudinal aging cohorts [11]. Thus, although offering viable developmental insights [14,21], previous lifespan studies of CT asymmetry do not accurately capture the aging process, and likely conflate non-linear developmental and aging trajectories with linear models. A longitudinal exploration of the lifespan trajectories of CT asymmetry accounting for dynamic change is needed to further knowledge of normal brain development.

In addition, few studies have charted developmental [31,33] or aging effects [8] on SA asymmetry. However, indirect evidence suggests SA asymmetry may exhibit little change from birth to 2 years [31] despite rapid and concurrent developmental cortical expansion [35] – suggesting SA asymmetry may be comparatively developmentally stable. Other evidence suggests SA asymmetries show little interindividual variation in directionality [8,33], whereas CT asymmetry may be more variable between individuals [8,33]. Additionally, SA asymmetry might reflect asymmetry in cortical minicolumns [36] whose microstructure is primarily determined early in fetal brain development [37,38]. Together with evidence genes associated with (predominantly) SA asymmetry show highest expression in prenatal life [39], this suggests a largely invariant [8,33,39] developmental plan of SA asymmetry *in utero* [31] that may show little change from birth to adulthood [8,31]. Determining the developmental timing and lifespan trajectories of asymmetry will provide a useful normative reference, as subtle alterations in cortical asymmetry in neurodevelopmental disorders suggest early life perturbations in left-right brain organization contribute to lifelong detriment in brain health [22,39].

Correlations between cortical asymmetries in adults may provide a window on asymmetries formed under common genetic-developmental influence. Yet while there has been much research on whether asymmetries of various morphometric measures [9,15,20] or imaging modalities [32] relate to one another, few have focused on interrelationships between asymmetries derived from the same metric [32,40]. Where reported, evidence suggests cortical asymmetries are mostly independent [41,42] – in line with a multifactorial view of asymmetry phenotypes [43–45] – and a recent study found asymmetry in anatomically connected regions of the cortical language network was no more related than in regions selected at random [32]. Currently, it is not known whether or how cortical asymmetries correlate within individuals, which may suggest coordinated development of left-right brain asymmetries.

Altered lateralization has been hypothesized to relate to poorer cognitive outcomes [21,46–48]. In line with this, recent work suggests genetic overlap between cortical asymmetry, educational attainment, and neurodevelopmental disorders [39], and reduced brain torque [30,49,50] – a gross morphological asymmetry with a strong population-level bias – associates with lower cognition [51]. For CT and SA asymmetry, however, reported asymmetry-cognition associations have been conflicting [21,52,53] and remain untested in large-scale data. Furthermore, most large-scale studies of the factors moderating cortical asymmetry have adopted brain atlases offering limited spatial precision [8,39,54]. Accordingly, previous large-scale studies did not detect associations with handedness [8,55] that were not found until a recent study applied vertex-wise mapping in big data [29]. Similarly, it is unclear to what degree poor-fitting atlases may drive down heritability estimates of cortical asymmetry [8,39,56,57], as estimates can be substantially higher when brain measures better conform to the biology under genetic investigation [56,57]. However, no previous study has tested heritability after precisely delineating the regions of cortex

that are asymmetric at the population level, and cortex-wide maps of asymmetry heritability have all used the same anatomical atlas we propose fits poorly to the asymmetry of cortex [26].

Here, we 1) delineate population-level cortical SA and CT asymmetries using vertex-wise analyses and their overlap in 7 international datasets, and 2) map the trajectories of population-level cortical asymmetries longitudinally across the lifespan. We then 3) investigate interregional asymmetry correlations, asking whether and how asymmetries correlate within individuals. Next, we 4) tested heritability of cortical asymmetry using both an extended twin design and genome-wide single nucleotide polymorphism (SNP) data. Finally, we 5) screened our set of robust, population-level asymmetries for association with general cognitive ability, handedness, sex, and brain size using large-scale biobank data [58].

2. Methods

2.1 Samples

We used anatomical T_1 -weighted (T_{1w}) scans from 7 independent international MRI datasets originating from 4 countries. See Table 1 for an overview of samples used for each analysis.

Sample (country)	Analysis	N unique	N obs (N longitudinal)	Mean follow-up interval (Range)	Age-range	Mean Age (SD)	Sex (F/M)
LCBC (Norway)	Reproducibility / Interrelationships	923	1572 (812)	2.7 (0.1-9.4)	18.0 - 55.0	30.6 (9.6)	622 / 301
	Lifespan trajectories	1886	3937 (2762)	2.7 (0.1-11)	4.1 - 89.4	36.8 (25.4)	1139 / 747
Cam-CAN (UK)	Reproducibility	321	321	-	18.5 - 54.9	38.7 (9.7)	171 / 150
DLBS (USA)	Reproducibility	160	160	-	20.6 - 54.9	37.5 (10.7)	98 / 62
SALD (China)	Reproducibility	301	301	-	19 - 54	33.7 (11.5)	191 / 110
IXI (UK)	Reproducibility	313	313	-	20.0 - 54.7	36.8 (9.6)	162 / 151
HCP (USA)	Reproducibility / Interrelationships	1111	1111	-	22 - 37	28.8 (3.7)	605 / 506
	Heritability*	1037	1037	-	22 - 37	28.9 (3.7)	570 / 467
UK Biobank (UK)	Reproducibility	1000	1000	-	46.1 - 55.0	52.1 (1.9)	581 / 419
	Interrelationships / Heritability** / Individual differences***	38172	38172	-	44.6 - 82.3	64.1 (7.6)	20138/18034

*Table 1: Demographics of the samples used for each analysis. The number of unique participants (N unique), total observations (N obs), and number of scans constituting longitudinal observations (N longitudinal) is shown. Note that only the LCBC sample included longitudinal data (70% longitudinal coverage). * See SI Table 1 for further details of the HCP extended twin design used for heritability analysis. ** For analyses of SNP-heritability and *** associations with individual differences, to maximize power to detect effects subsets based on maximum data availability were taken from the UK Biobank base sample described (i.e., all individuals with genotype data surpassing quality control; all individuals with available cognitive/handedness data; see 2.3.4 and 2.3.5).*

2.1.1 Datasets: Reproducibility across samples

To delineate average adult patterns of whole-cortical SA and CT asymmetry, we restricted the age-range of all samples used in the vertex-wise analyses to 18-55 (see Table 1). ***Dataset 1*:** Here, the Center for Lifespan Changes in Brain and Cognition (*LCBC*) sample comprised 1572 mixed cross-sectional and longitudinal scans (N longitudinal = 812; timepoint range = 1-6) from 923 unique participants (mean age = 30.6 ± 9.6) collected across 2 different scanners. Additionally, 125 individuals were double-scanned at the same timepoint on both scanners. ***Dataset 2:*** The Cambridge Centre for Ageing and Neuroscience (*Cam-CAN*) [59] sample comprised cross-sectional scans of 321 individuals (mean age = 38.7 ± 9.7) [60]. ***Dataset 3:*** The Dallas Lifespan Brain Study (*DLBS*) [61] sample comprised cross-sectional scans of 160 individuals (mean age = 37.5 ± 10.7). ***Dataset 4:*** The Southwest University Adult Lifespan Dataset (*SALD*) [62] sample comprised cross-sectional scans of 301 individuals (mean age = 33.7 ± 11.5). ***Dataset 5:*** The *IXI* sample comprised cross-sectional scans of 313 healthy individuals collected on three different scanners (mean age = 36.8 ± 9.6; see http://brain-development.org/ixi-dataset). ***Dataset 6:*** Here, the Human Connectome Project (*HCP*) 1200 [63] sample comprised 1111 scans (mean age = 28.8 ± 3.7; see also section 2.1.3.). ***Dataset 7:*** Here, the UK Biobank sample (application #32048) consisted of 1000 randomly sampled cross-sectional scans meeting age-range criteria (mean age = 52.1 ± 1.9), restricted to be comparable in size to the other datasets in this analysis. Note that with the exception of vertex-wise analyses in UK Biobank, all vertex-wise analyses made use of all available scans from each sample meeting the age-range criteria.

2.1.2 Dataset: Lifespan trajectories

To characterize the lifespan trajectories of cortical asymmetry, we used the full age-range of the LCBC dataset (4.1 - 89.4 years), with a sample comprising 3937 cross-sectional and longitudinal scans (N longitudinal = 2762; females = 1139; mean age = 36.8) from 1886 unique individuals collected across 4 scanners (including all observations used in the reproducibility analysis). Here, 271 scans were double-scans (see above). The full LCBC lifespan dataset has been described elsewhere [64,65].

2.1.3 Datasets: Interregional correlations

We used the three largest datasets to assess and replicate covariance patterns between cortical asymmetry phenotypes within individuals; LCBC (N = 923; N obs = 1572; see Table 1), HCP (N = 1109) and the full UK Biobank imaging sample (N = 38,172).

2.1.4 Datasets: Heritability and individual differences

Extended twin design. For heritability analyses, we used the publicly available HCP 1200 sample. HCP subjects were recruited from the Missouri Family and Twin registry, and individuals primarily forming young adult sibships – including sets of monozygotic (MZ) and dizygotic (DZ) twins – were selected for participation [63]. For heritability analysis, we made use of 1037 scans from twins and non-twin siblings (age-range = 22-37; mean age = 28.9 ± 3.7). All included twin pairs were same-sex. The various kinships are described in SI Table 1. ***SNP-heritability***. Full UK Biobank imaging sample with genome-wide data surpassing quality control (N = 31,433; see 2.2.5).

Individual differences: Full UK Biobank imaging sample subsetted by the number of available observations for each variable-of-interest (see 2.2.6).

2.2. MRI acquisition and preprocessing

MRI acquisition parameters for all samples are summarized in SI Table 2. $T1_W$ anatomical images were processed with FreeSurfer's cross-sectional pipeline (v6.0.0) [66] and vertex-wise SA and CT morphometry estimates were obtained for each MRI observation. Briefly, the FreeSurfer pipeline includes steps such as removal of non-brain tissue, Talairach transformation, intensity normalization, demarcating the grey/white and grey/CSF boundaries, cortical surface reconstruction and parcellation [26,67]. As the LCBC sample also contained longitudinal observations, initial cross-sectional reconstructions in LCBC were subsequently ran through FreeSurfer's longitudinal pipeline. This uses robust inverse consistent registration to and common information from an unbiased within-subject template to initialize several of the aforementioned processing steps and increase reliability of cortical morphometry estimates [68].

SA and CT maps of the left hemisphere (LH) and right hemisphere (RH) of each participant in each dataset were resampled from the native cortical geometry to a high-resolution symmetrical surface template ("*LH_sym*"; https://www.gin.cnrs.fr/en/tools/lh-sym) [15,69] based on cross-hemispheric registration using FreeSurfer "Xhemi" routines [70]. This procedure achieves vertex-wise alignment of the data from each participant and homotopic hemisphere in a common analysis space. SA values were resampled with an added Jacobian correction to account for stretching or compression during registration, ensuring preservation of the areal quantities [71]. In symmetric space, we then applied an 8 mm full-width half-maximum Gaussian kernel to surface-smooth the LH and RH data.

2.3 Data analysis

2.3.1 Reproducibility across samples: population-level asymmetry

All analyses were performed in FreeSurfer (v6.0) and R (v 4.0.0). First, for each of the 7 datasets we assessed SA and CT asymmetry vertex-wise using FreeSurfer's Linear Mixed Effects (LME) tool [72]. LME provided a common analysis framework to model both the mixed-effects LCBC sample and the repeated measures cross-sectional samples. Asymmetry was delineated via the within-subject main effect of Hemisphere, covarying for the fixed effects of Age, Age × Hemisphere, Sex, Scanner (where applicable), with a random subject term. Correction for multiple comparisons was performed using FreeSurfer's powerful 2-stage False Discovery Rate (FDR) procedure (corrected at p[FDR] < .005) [72]. For each sample and cortical metric, we computed maps of the mean Asymmetry Index (AI; defined here as (LH-RH) / ((LH+RH)/2). Spatial overlap of the unthresholded AI maps across datasets was quantified using Pearson's r. Next, to identify cortical regions exhibiting robust SA and CT asymmetry effects across datasets, we thresholded and binarized the mean AI maps by a given (absolute) effect size (SA = 5%; CT = 1%; achieving p[FDR] < .005 in most datasets), and summed the binary maps. After removing the smallest clusters (<200 mm^2), a set of robust asymmetry clusters was defined as those exhibiting overlapping effects in 6 out of 7 independent samples. We then extracted SA and CT data in symmetrical space for each cluster, subject, and hemisphere, spatially averaging across vertices within the cluster. These robust clusters – exhibiting population-level SA and CT asymmetry – were used in subsequent analyses.

2.3.2 Lifespan trajectories of population-level cortical asymmetries

We have recently shown that cortical regions exhibiting age-related reduction of CT asymmetry correspond with regions exhibiting strong asymmetry on average [11]. Thus, having delineated clusters exhibiting population-level SA and CT asymmetry, we aimed to characterize the trajectories of SA and CT asymmetry across the lifespan (4-90 years) using a longitudinal dataset. As lifespan trajectories are often non-linear, a flexible modelling approach is recommended for the assessment of lifespan trajectories [73]. Thus, we used a factor-smooth Generalized Additive Mixed Model (GAMM) approach ("gamm4" R package [74]) that allowed modelling the smooth LH and RH age-trajectories within our robust clusters. Here, we fit a smooth age trajectory per hemisphere, and assessed the smooth Age × Hemisphere interaction to determine whether and how cortical asymmetries change with age. The linear predictor matrix of the GAMM was used to obtain asymmetry trajectories and their confidence intervals, computed as the difference between zero-centered (i.e. demeaned) hemispheric age-trajectories. We included Hemisphere as an additional fixed effect, sex and scanner as covariates-of-no-interest, and a random subject intercept. A low number of basis dimensions for each smoothing spline was chosen to guard against overfitting (knots = 6). For this analysis, outliers defined as observations falling > 6SD from the trajectory of either hemisphere were removed on a region-wise basis.

2.3.3 Interregional asymmetry correlations

To investigate whether and how cortical asymmetry correlates within individuals, we assessed the covariance between clusters exhibiting population-level asymmetry, separately for SA and CT. Here, we regressed out the fixed effects of age,

sex and (where applicable) scanner from each AI using linear models, and obtained a cluster-cluster correlation matrix (Pearson's *r*) for all leftward and rightward cluster AI's, after inversing all individual AI's in clusters with rightward mean asymmetry to be positive (such that positive correlations denote positive asymmetry-asymmetry relationships regardless of the direction of mean asymmetry in the cluster). Replication was assessed using the Mantel test ("ade4" R package [75]), which assesses the similarity/correlation between two matrices. For SA and CT, distance matrices were obtained from the correlation matrices derived separately from LCBC, HCP and UK Biobank data (the three largest datasets), and matrix similarity was tested between each dataset-pair across 10,000 permutations. At this point, two very strong outliers in HCP data were detected and discarded for all subsequent analyses (SI Fig. 7). Based on the results, we post-hoc tested whether the covariance between asymmetries was related to proximity in cortex. For this, we obtained the average geodesic distance between all pairs of leftward and rightward clusters on the cortical surface (i.e. opposite-hemisphere geodesic distance) using the "SurfDist" Python package (https://github.com/NeuroanatomyAndConnectivity/surfdist) [76], and correlated pair-wise distance with the pair-wise correlation coefficient (Fisher's transformed coefficients; Spearman's correlation). For CT, to assess whether the observed covariance patterns reflected a global factor for CT asymmetry, we performed post-hoc principal components analysis (PCA) across z-transformed AI's for all CT asymmetry clusters after correcting each for age, sex and (if applicable) scanner. Based on these results, we computed the mean AI across all leftward clusters and across all rightward clusters (means weighted by cluster size and corrected for the same covariates), and tested the partial correlation between mean leftward CT asymmetry in left-asymmetric clusters and mean rightward CT asymmetry in rightward-asymmetric clusters in each of the three cohorts.

2.3.4 Heritability

Heritability of SA and CT asymmetry was assessed using both twin- and SNP-based methods, both for the set of robust asymmetry clusters and cortex-wide using a detailed parcellation scheme (500 parcels) [77]. For cluster analyses, significance was considered at Bonferroni-corrected p<.05 applied separately across sets of robust SA and CT clusters (14 SA, 20 CT). For whole cortical mapping, significance was considered at *p(FDR)* < .05 applied across the parcellation scheme for each metric (500 tests per SA and CT map).

Extended twin design: In HCP, heritability for each AI measure was assessed using the "OpenMx" R package [78], a structural equation modeling program based on maximum-likelihood estimation. We used a variance-component decomposition method to estimate heritability: the classical ACE model. Using observed cross-twin and cross-sibling covariance, the ACE model decomposes the proportion of observed phenotypic variance into additive genetic effects [A], shared environmental effects [C], and unique environmental effects and/or error [E] [78]. Data were reformatted such that rows represented family-wise observations. As is standard, we set A to be 1 for MZ twins assumed to share 100% of their segregating genes (but see [79]), 0.5 for DZ twins and siblings that share 50% on average, and shared environment was assumed equal for twins and non-twin siblings (but see [80,81]). Prior to estimating heritability, for each phenotype we regressed out the effects of age and sex via linear models and computed z-scores. Statistical significance of genetic and shared environment effects was assessed by comparing ACE model fit to submodels with the parameter-of-interest removed.

SNP-heritability: The final genetic sample consisted of 31,433 UK Biobank participants (application #32048) from our imaging sample included in the "white British ancestry" genetic subset [data field 22006] [82] with quality checked genetic data. Details for sample collection and genotyping can be found at https://biobank.ndph.ox.ac.uk/). We removed subjects that were outliers based on heterozygosity [22027] and missingness (rate > 0.05), mismatched genetic and self-reported sex [22001], sex chromosome aneuploidies [22019], and those not in the "white British ancestry" genetic subset [82]. At the variant level, after removing SNPs with minor allele frequency < 0.01, genotype data from 654,584 autosomal SNPs were used to compute a genetic relationship matrix using GCTA software (v1.93.2) [83]. For each phenotype, we first regressed out the effects of age and sex via linear models and computed z-scores. Genome-based restricted maximum likelihood (GREML) methods as implemented in GCTA were then used to compute SNP-heritability for each AI measure, applying a kinship coefficient cut-off of 0.025 (excluding one individual from each pair), and controlling for genetic population structure (first ten principal components). Bivariate GREML analysis was employed to test genetic correlations between asymmetry in our set of robust clusters [83], with pair-wise relationships tested only for cluster-pairs where both clusters in a pair exhibited significant SNP-heritability (p < .05; pre-corrected). Significance of genetic correlations was assessed at *p(FDR)* <.05.

2.3.5 Associations with Cognition, Sex, Handedness, & ICV

Finally, we assessed the relationships between asymmetry in our robust asymmetry clusters and general cognitive ability, handedness, sex and estimated intracranial volume (ICV) using linear models in UK Biobank. For cognition, we used the first principal component (PC1) across the following 11 core cognitive variables in UK Biobank [84]: Mean reaction time [data field 20023] (log transformed), Numeric memory [4282], Fluid reasoning [20016], Matrix completion [6373], Tower rearranging [21004], Symbol digit substitution [23324], Paired associate learning [20197], Prospective memory [20018], Pairs matching [399], Trail making A [6348], Trail making B [6350]. Prior to the PCA, for participants with available cognitive data, data was imputed for missing cognitive variables via the "imputePCA" R function (number of estimated components tentatively optimized using general cross validation; "missMDA" Package [85]). PC1 (explaining 38.2%; SI Table 9) was inversed to correlate negatively with age (r = -.36), ensuring higher values reflected higher cognition. As fewer participants had cognitive data relative to the other variables, for each cluster we ran one set of linear models to assess the marginal effect of cognition (PC1 as predictor; age, sex, ICV controlled; N = 35,199), and one set of linear models to assess the marginal effects of Handedness, Sex, and ICV in a model including all three predictors (age controlled, N = 37,570; number of participants in UK Biobank base sample with available handedness data). For the cognitive analysis, effects identified in the imputed dataset were checked against the confidence intervals for the effect in the subset of the data with no missing cognitive variables (N = 4696). Participants who self-reported as mixed handed were not included as this self-report can be unreliable over repeat time-points [29]. Significance was considered at Bonferroni-corrected $\alpha = p < 7.3^{-5}$ (.01/136 [34

clusters × 4]).

3. Results

3.1 Population-level asymmetry of the cerebral cortex

SA asymmetries were markedly consistent across all 7 datasets (see Fig.1A for effects): the spatial overlap between AI maps ranged from *r* = .89 to .97 (Fig. 1B). Across all datasets (Fig 1C), strong leftward SA asymmetry was observed in a large cluster in supramarginal gyrus (SMG) that spanned the length of postcentral gyrus, extended inferiorly into PT and primary auditory regions in the Sylvian fissure, and conformed markedly to their anatomical boundaries (see SI Fig.1A for significance). Strong leftward SA asymmetry was also consistently observed in anterior insula, anterior temporal cortex, rostral anterior cingulate, medially in superior frontal cortex, and precuneus, the latter extending the length of parahippocampal gyrus into entorhinal cortex. Strong rightward SA asymmetry was consistently evident in cingulate cortex, inferior parietal cortex, STS, lateral and medial occipital cortex, and in mPFC and rostral middle frontal cortex (Fig. 1A). Effects showed markedly high overlap across datasets (Fig. 1C), and the global pattern agrees with previous reports [8,25,29,86].

For CT, an anterior-posterior pattern of left-right asymmetry was evident in most datasets (see Fig. 2A for effects), consistent with more recent reports [8,11,29]. Though spatial correlations between AI maps were generally high between most datasets, they were notably more variable (range *r* = .33 - .93; Fig. 2B); HCP showed lower correlation with all datasets (*r* = .33 - .46) whereas all other datasets correlated highly with each other (min *r* = .78). Strong leftward CT asymmetry was evident in cingulate cortex, postcentral gyrus, and in superior frontal cortex – with consistent effects across datasets (Fig. 2C) – and in medial and lateral prefrontal cortex, though the latter two were less consistent among datasets. Strong rightward CT asymmetry was consistently observed in a large cluster in and around STS (Fig 2C) encompassing most of lateral temporal cortex and extending posteriorly into lateral occipital, and superiorly into PT and auditory processing regions in the Sylvian fissure (see SI Fig. 1B for significance). Strong rightward CT asymmetry was also consistently evident in insula, lingual gyrus, anterior parahippocampal and entorhinal cortex. Of note, both SA and CT asymmetry extended beyond these described effects (SI Fig.1).

Based on effect size criteria (as shown in Figs. 1 & 2 and described in 2.3.1), we derived a set of clusters exhibiting population-level asymmetry for SA (14 clusters; Fig. 1C) and CT (20 clusters; Fig. 2C) to be used in further analyses (see Tables 2 & 3 for anatomical descriptions, see SI Fig 2 for variances). We then formally compared our approach to asymmetry estimates derived from the Desikan-Killany (DK) parcellation, a gyral-based cortical atlas often used for the assessment of cortical asymmetry [8,20,39,87], finding fairly poor anatomical correspondence for DK parcels to the vertex-wise structure of cortical asymmetry, particularly for CT (see SI; SI Fig. 4).

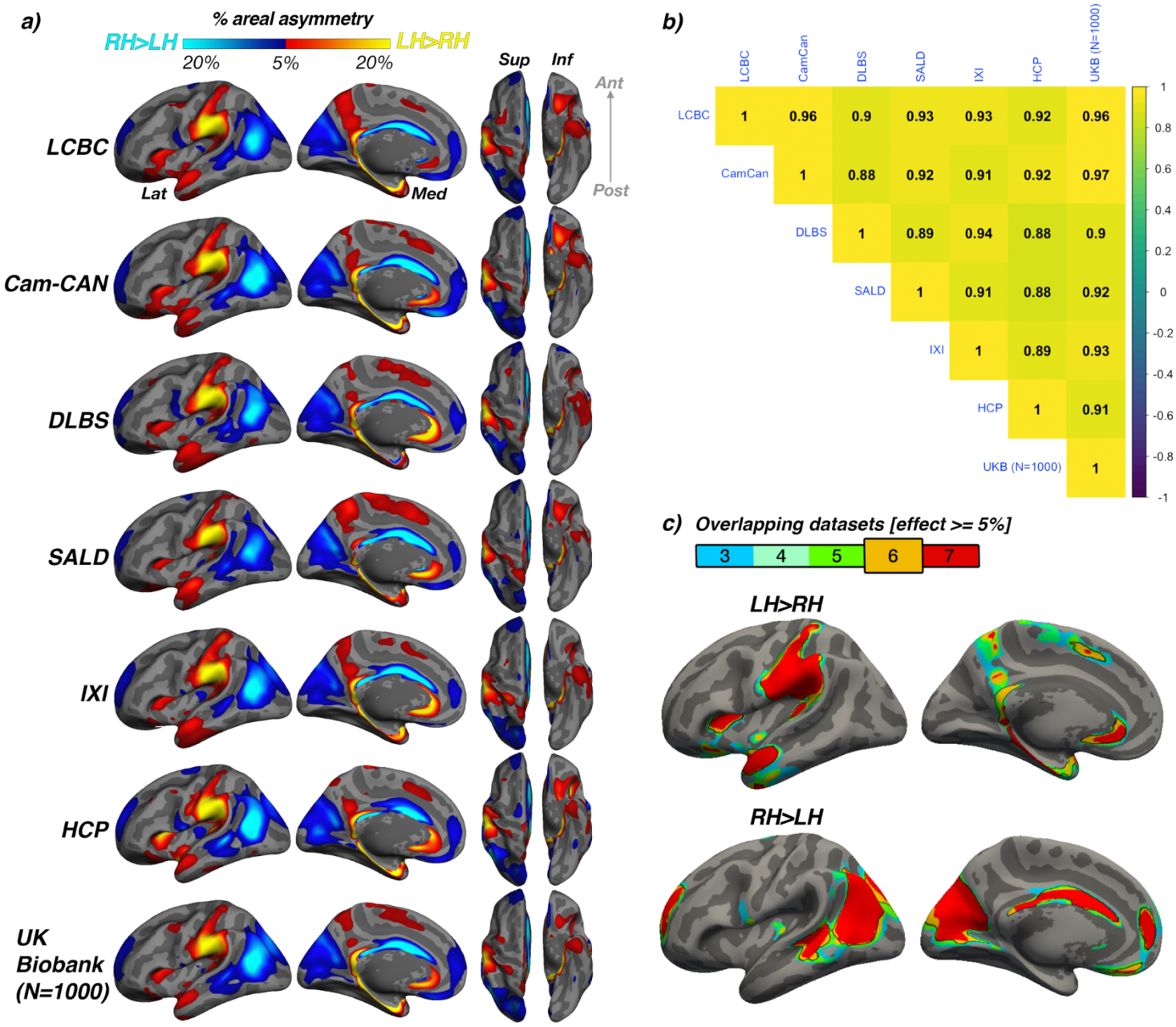

Figure 1. A) *Mean SA asymmetry for each dataset. All maps available at neurovault.org/XXXX. Warm and cold colours depict leftward and rightward asymmetry (in %), respectively.* ***B)*** *Correlation matrix (Pearson's r) depicting the spatial overlap of the unthresholded effects between datasets.* ***C)*** *Overlap in effects across datasets (lower threshold = 5%) was used to delineate a set of robust clusters exhibiting population-level SA asymmetry based on a minimum 6-dataset overlap (black outlined clusters). Post=posterior; Lat=lateral; Med=medial; Ant=anterior; Sup=superior; Inf=inferior.*

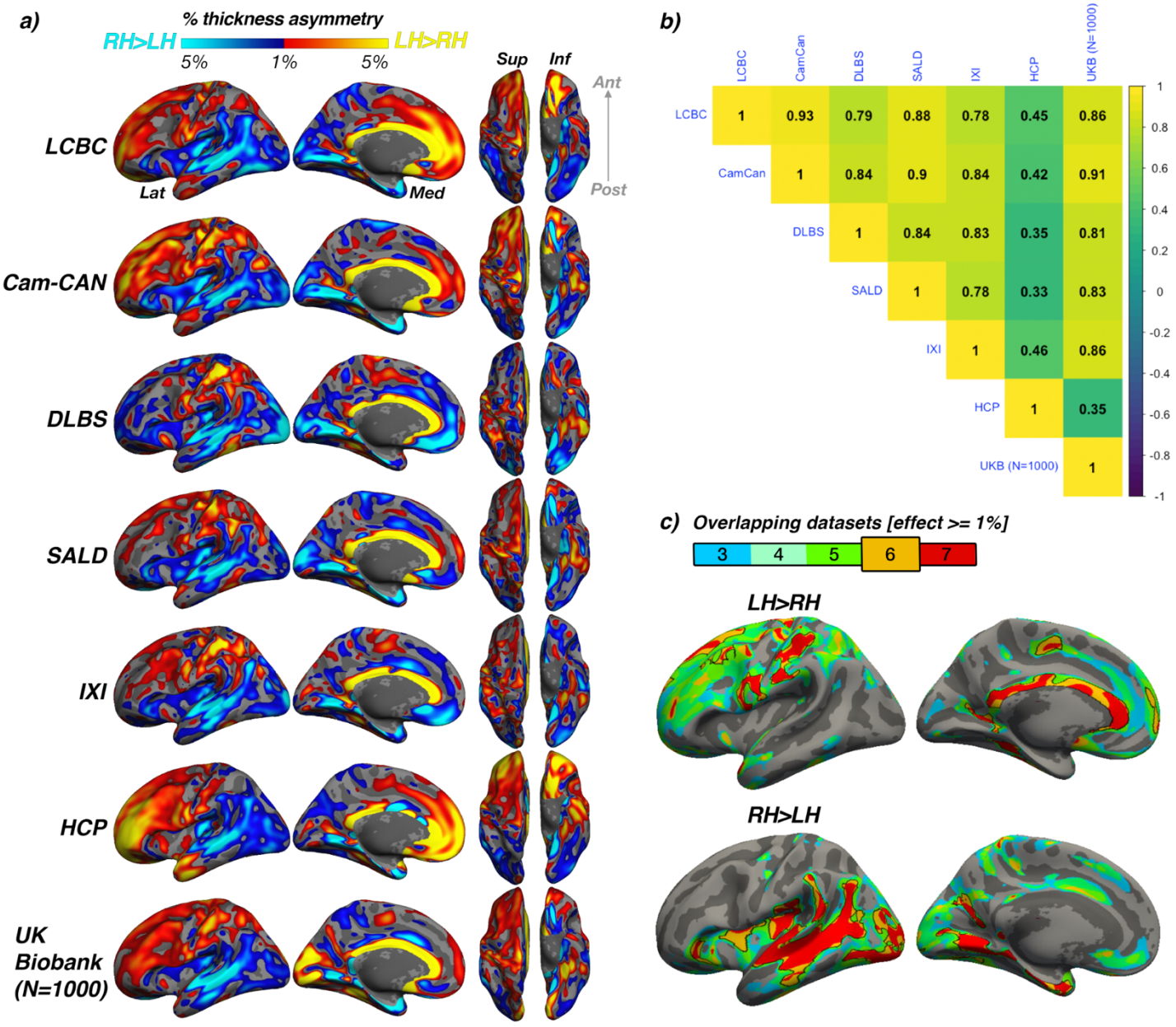

***Figure 2**. **A)** Mean CT asymmetry for each of the 7 datasets. All maps available at neurovault.org/XXXX. Warm and cold colours depict leftward and rightward asymmetry (%), respectively. **B)** Correlation matrix (Pearson's r) depicting the spatial overlap of unthresholded effects between datasets. **C)** Overlap in effects across datasets (1% lower threshold) was used to delineate a set of robust clusters exhibiting population-level CT asymmetry based on a minimum 6-dataset overlap (black outlined clusters).*

3.2 Lifespan trajectories of cortical asymmetry

Homotopic lifespan trajectories in clusters exhibiting population-level SA asymmetry are shown in Fig. 3 (see SI Fig.5A for asymmetry trajectories). In all clusters, SA asymmetry was strongly established already by age ~4 years, and the lifespan trajectories of both leftward (Fig 3A) and rightward (Fig 3B) SA asymmetries were largely parallel. Specifically, a large left asymmetric cluster encompassing SMG, postcentral gyrus and perisylvian cortex (#1; Fig. 3) showed strong asymmetry by age ~4 that was maintained throughout life through steady aging-associated decline of both hemispheres, whereas leftward asymmetry of temporal cortex (#2,6) and anterior insular (#4) was maintained through developmental expansion and age-associated decline of both hemispheres. Others (retrosplenial #5; mPFC #3,7) showed growth from pre-established asymmetry and more variable lifespan trajectories. On the other side, rightward clusters showed largely preserved asymmetry through aging-associated decline of both hemispheres (Fig 3B; medial occipital #1; lateral parietal #2; STS #5; orbitofrontal cortex #7), through bilateral developmental expansion and aging-associated decline (mPFC #6), or steadily expanding bilateral SA until mid-life (cingulate; #3). Though asymmetry trajectories did show significant change at some point throughout life in most clusters (SI Table 4), factor-smooth GAMM interaction analyses (SI Fig. 5A) confirmed that asymmetry was significantly different from 0 across the entire lifespan in all SA clusters, and the average trajectories

across all leftward and rightward clusters were clearly parallel (bordered plots in Fig. 3; though still exhibited a significant difference; see SI Table 4).

In contrast, though homotopic trajectories of CT clusters were more variable, they were mostly characterized by developmental increase and aging-associated decrease in asymmetry (i.e. non-parallel lifespan trajectories), through unequal rates of continuous thinning between the hemispheres from age ~4 (Fig. 4; see also SI Fig. 5B). Specifically, leftward CT asymmetry developed through comparatively slower thinning trajectories of the LH, whereas rightward asymmetry developed through slower RH thinning. In general, asymmetry development was evident up to a peak around age ~25 for both leftward (Fig. 4; superior frontal #2; precentral #4, frontal #8,9,10; calcarine #11) and rightward clusters (#1-9) and declined thereafter. Factor-smooth GAMMs (SI Fig. 5B) confirmed that the developmental foundation for CT asymmetry was already established by age ~4 (95% of CT clusters exhibited small but significant asymmetry at age ~4; SI Fig.5B), and again asymmetry trajectories showed significant change at some point throughout life (SI Table 5). The average trajectories across all leftward and rightward clusters showed developmental asymmetry increase up to age ~25 and age-associated asymmetry decrease around age 50 (bordered plots; Fig 4). SA and CT results were robust to varying the number of knots used to estimate hemispheric trajectories (see SI Fig. 6).

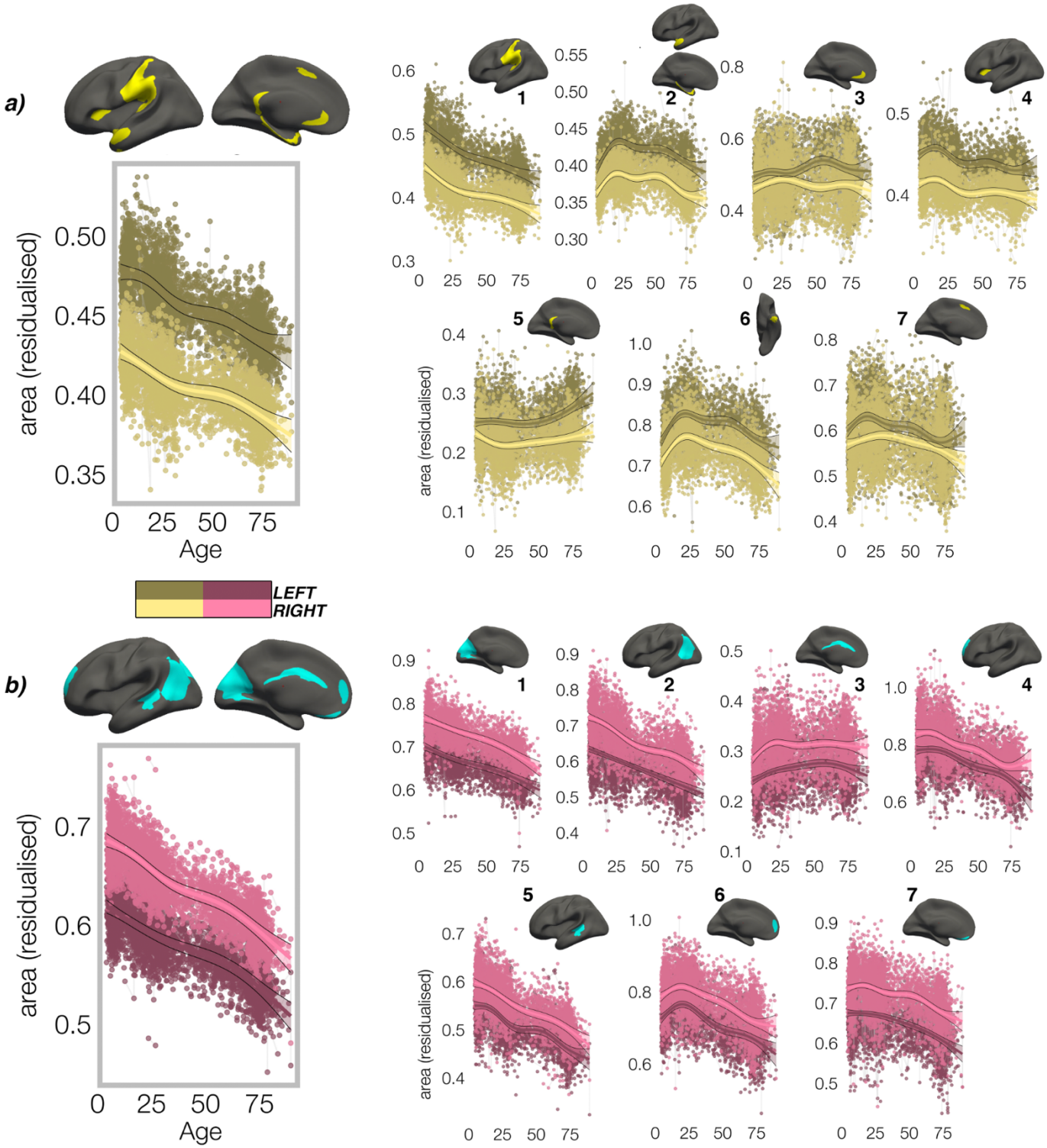

Figure 3: *Homotopic lifespan trajectories in clusters exhibiting population-level* ***a)*** *leftward (yellow plots; yellow clusters) and* ***b)*** *rightward (pink plots; blue clusters) areal asymmetry (mm^2). Larger plots on the left show the mean age trajectory across all clusters exhibiting leftward (top) and rightward (bottom) asymmetry. Note that the unit of measurement is the average surface area of a vertex within the cluster. Dark colours correspond to LH trajectories. All age trajectories were fitted using GAMMs. Data is residualized for sex, scanner and random subject intercepts. Clusters are numbered for reference.*

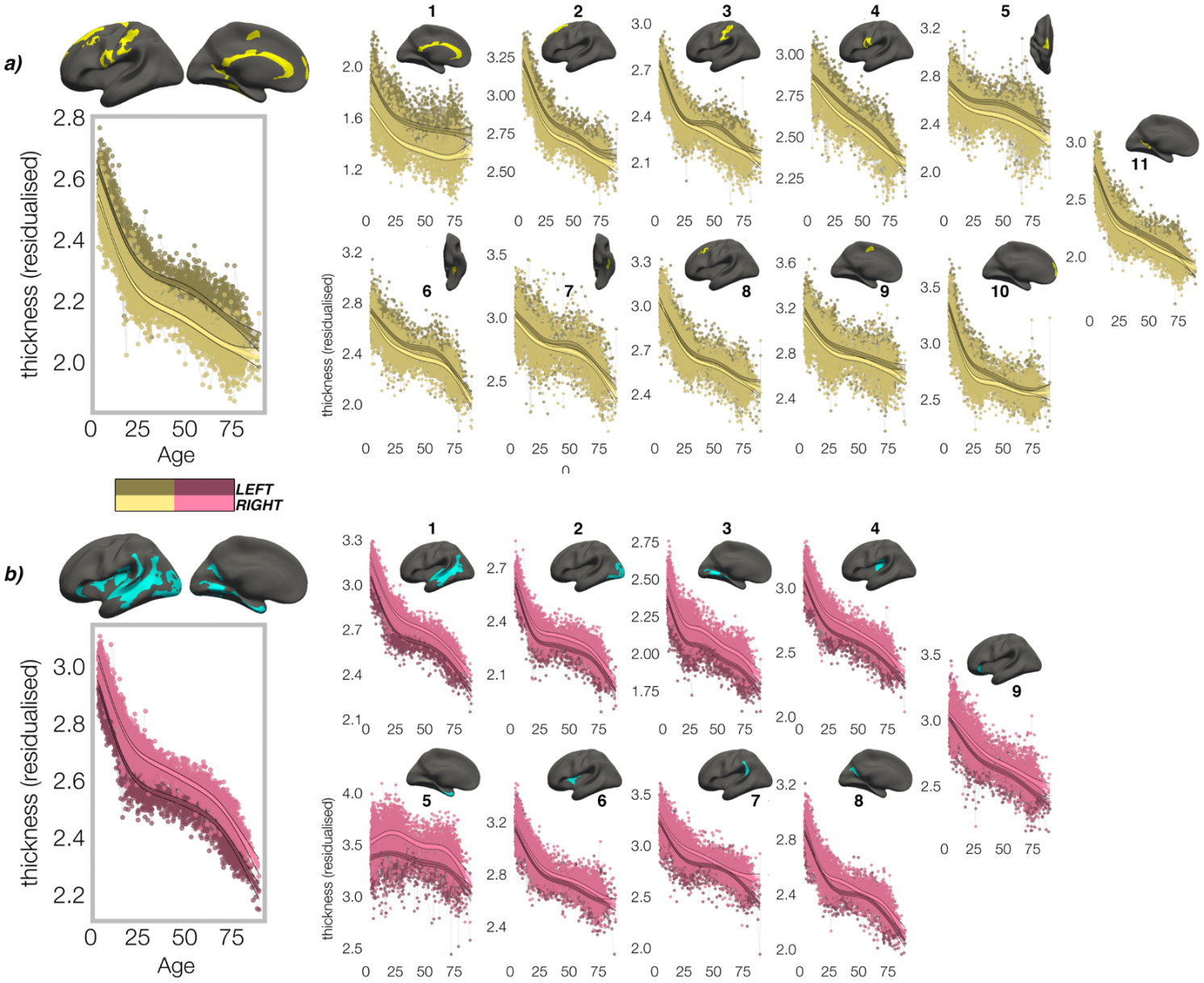

Figure 4: *Homotopic lifespan trajectories in clusters exhibiting population-level* ***a)*** *leftward (yellow plots; yellow clusters) and* ***b)*** *rightward (pink plots; blue clusters) thickness asymmetry (mm). Larger plots on the left show the mean age trajectory across all clusters exhibiting leftward (top) or rightward (bottom) asymmetry. Dark colours correspond to LH trajectories. All age trajectories were fitted using GAMMs. Data is residualized for sex, scanner and random subject intercepts. Clusters are numbered for reference.*

3.3 Interregional asymmetry correlations

For SA asymmetry, covariance between population-level asymmetries was highly consistent between datasets: LCBC, UK Biobank and HCP all correlated almost perfectly (r >= 0.97, all $p < 10^{-5}$), indicating a common covariance structure was detectable across datasets (Fig. 5A; annotated matrices in SI Fig. 8). Interestingly, the highest correlations (or "hotspots") all reflected positive correlations between regions that are on average left-asymmetric and regions that are on average right-asymmetric in the population (i.e. higher leftward asymmetry in one region related to higher rightward asymmetry in another; Fig 5A; black outline); leftward asymmetry in SMG/perisylvian (#1L) was related to higher rightward asymmetry in inferior parietal cortex (#2R; r = .46 [LCBC]), leftward asymmetry in anterior cingulate (ACC; #3L) was strongly related to higher rightward asymmetry in mPFC (#6R, r = .46 [LCBC]), and higher leftward asymmetry in a small superior frontal cluster (#7L) was strongly related to higher rightward asymmetry of the cingulate (#3R, r = .67 [LCBC]). Importantly, none of the relationships could be explained by brain size, as additionally removing the ICV-associated variance from cluster AI's had a negligible effect on their interrelations (max single correlation change in any dataset-pair = 0.008). Post-hoc tests confirmed that opposite-direction asymmetries were more correlated if closer in cortex; geodesic distance (i.e. here the distance between regions exhibiting leftward asymmetry and rightward asymmetry along the ipsilateral surface) was lower between cluster-pairs that were more correlated (*rho* = -.37, p = .01 [LCBC]; *rho* = -.38; p = 007 [UK Biobank; Fig. 5B]; *rho* = -.32; p = .02 [HCP]), though this relationship was mainly driven by the aforementioned "hotspots". By contrast, same-direction (i.e. within-hemisphere) regional asymmetries were not more correlated if closer in cortex (leftward [all p > .5]; rightward [all p > .5]). This suggests that specific SA asymmetries that are closer in cortex and opposite in direction may track together within individuals during development.

For CT asymmetry, the correlation matrix exhibited a clear pattern in UK Biobank that was less visible but still apparent in LCBC and HCP (Fig. 5C). Mantel tests confirmed that the covariance structure replicated between all dataset-pairs (LCBC-HCP r = .45, p = .006; LCBC-UK Biobank r = .43, p = .01; UK Biobank-HCP r = .46, p = .01). The observed pattern suggested higher leftward asymmetry in regions that are on average left asymmetric in the population was associated with less rightward asymmetry in regions that are on average right asymmetric in the population. However, given that the AI measure is bidirectional, closer inspection of the correlations revealed that higher leftward asymmetry in regions that are left-asymmetric in fact corresponded to more *leftward* asymmetry in right-asymmetric regions, and vice versa (and on average; see SI Fig. 9). In other words, the observed covariance patterns suggest CT asymmetry is globally interrelated across cortex, and that individuals may tend towards either leftward lateralization or rightward lateralization (or symmetry) on average, irrespective of the region-specific direction of mean asymmetry in the cluster. Similarly, asymmetry in left-asymmetric regions was mostly positively correlated, and asymmetry in right-asymmetric regions was mostly positively correlated. Again, additionally removing ICV-associated variance had negligible effect (max single correlation change = 0.007). A post-hoc PCA analysis in UK Biobank revealed PC1 explained 21.9% of the variance in CT asymmetry and strongly suggested a single global factor for CT asymmetry (Fig. 5D). Accordingly, we observed a strong correlation between mean asymmetry across all leftward clusters vs. mean asymmetry across all rightward clusters (AI's inversed; weighted means) in UK Biobank (r = .61; $p < 10^{-16}$; Fig. 5D). Though less strong, these relationships were significant in both LCBC (r = -.10; $p = 1.3^{-4}$) and HCP (r = -.10; $p = 1.7^{-4}$), and there was evidence for a principal component for CT asymmetry in each (SI Fig. 10). Opposite-direction CT asymmetries that were closer in cortex were more negatively correlated in LCBC (*rho* = .29, p = .004) but not HCP (p = .33) or UK Biobank (p = .84), whereas CT asymmetry in left- (*rho* = -.44 [LCBC]; *rho* = -.44 [UK Biobank], *rho* = -.29 [HCP], all p < .05) and right- (*rho* = -.34 [LCBC]; *rho* = -.49 [UK Biobank], *rho* = -.57 [HCP]; all p < .05) asymmetric regions was more positively correlated in cluster-pairs that were closer in cortex. Overall, these results suggest that CT asymmetry is globally interrelated across the cortex and shows high directional variability in the adult population.

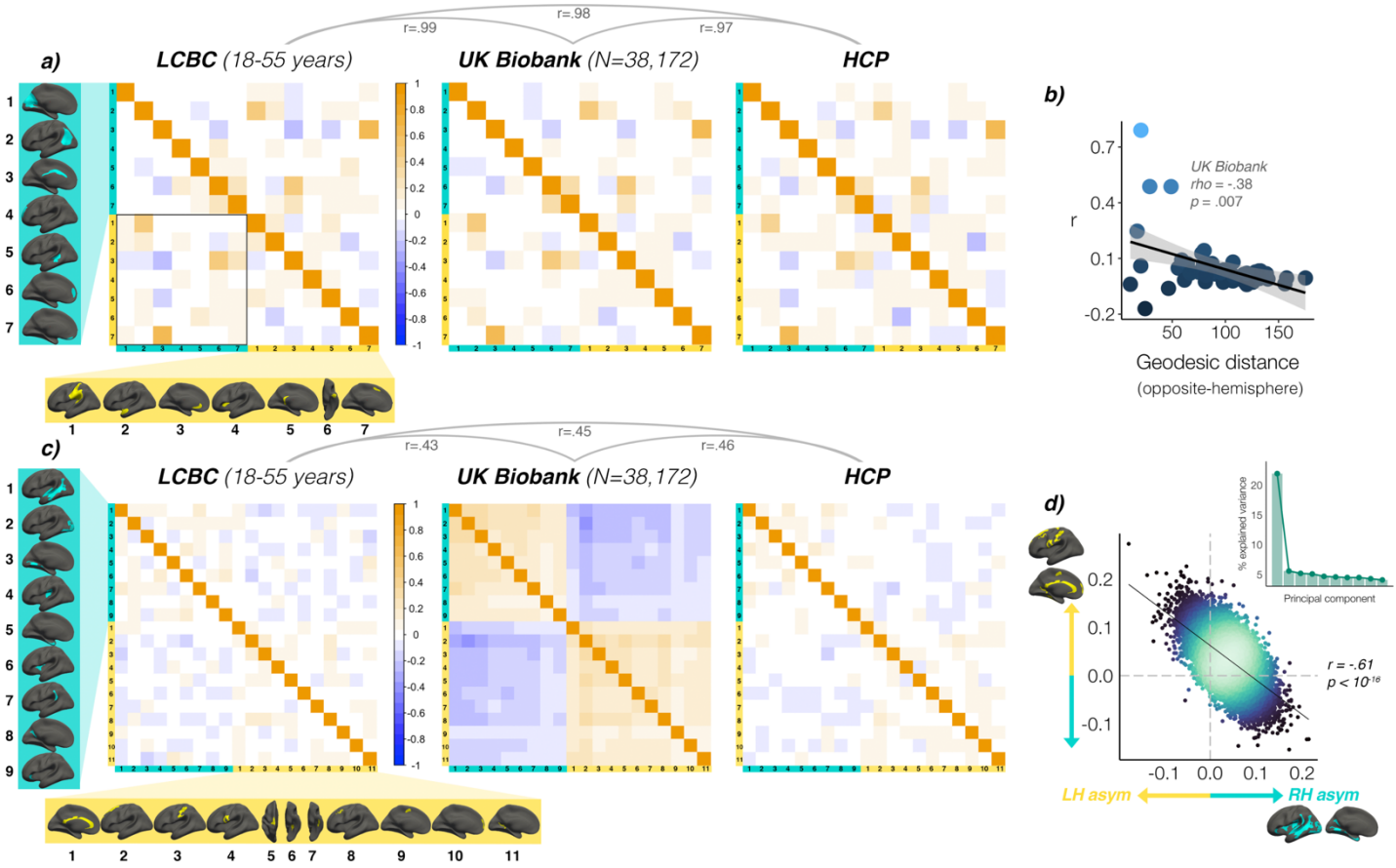

Figure 5: *Interregional correlations between population-level asymmetries exhibiting* ***A)*** *SA asymmetry and* ***C)*** *CT asymmetry for each adult replication dataset (AI's residualized for age, sex, scanner). AI's in rightward clusters are inversed, such that positive correlations denote positive asymmetry-asymmetry relationships regardless of direction. Yellow and blue brain clusters/colours denote population-level leftward and rightward asymmetries, respectively (clusters numbered for reference). Covariance structures were highly consistent across replication datasets for SA asymmetry (****A****; r >= .97) and CT asymmetry (****C****; r >=.43), as revealed by pair-wise whole-matrix comparisons (Mantel tests; results shown above matrices). Black box in A highlights the relationships between opposite-direction asymmetries in different regions of cortex (i.e. leftward v rightward regions).* ***B)*** *Datapoints represent leftward vs. rightward cluster-pairs. For SA, a significant negative correlation confirmed the impression that opposite-direction cluster-pairs that were closer in cortex (i.e. geodesic distance) were more positively correlated (y-axis).* ***D)*** *PCA analysis across AI's in all leftward and rightward CT clusters revealed a single component explained 21.9% of the variance in CT asymmetry in UK Biobank (inset plot). Accordingly, a strong correlation ($r = -.61$; $p < 10^{-16}$) was observed in UK Biobank between mean asymmetry across all leftward clusters (Y-axis) vs. mean asymmetry across all rightward clusters (X-axis; AI's inversed; means weighted by cluster size). Lines of symmetry (0) are shown in dotted grey. Similar results were obtained for LCBC and HCP (SI Fig. 10).*

3.4 Heritability

			HCP (extended twin)						UK Biobank (SNP-based)	
Direction	**ROI #**	**Cluster**	*h2*	*p*	*c2*	*e2*	*-2LL ACE*	*-2LL CE*	*h2 [± 95% CI]*	*p*
Leftward	1	L_Postcentral-gyrus_Supramarginal	0.246 (0 - 0.37)	0.177	0.009	0.745	2918.6	2920.5	**0.107** (0.07-0.144)	**3.01E-09**
	2	L_Anterior-temporal_Parahippocampal-gyrus	0 (0 - 0.129)	1	0.048	0.952	2938.8	2938.8	**0.063** (0.026-0.10)	**4.47E-04**
	3	L_Anterior-cingulate_Subcallosal	0.079 (0 - 0.205)	0.647	0.011	0.91	2937.6	2937.8	**0.048** (0.012-0.085)	**4.46E-03**
	4	L_Anterior-insula	0.207 (0.102 - 0.314)	0.222	0	0.793	2925.1	2926.6	[1] **0.186** (0.149-0.224)	**0.00E+00**
	5	L_Retrosplenial-cortex	0 (0 - 0.101)	1	0.01	0.99	2940.8	2940.8	**0.093** (0.056-0.13)	**2.57E-07**
	6	L_Temporal-pole_Inferior-temporal-gyrus	0.126 (0 - 0.243)	0.092	0	0.874	2935.8	2938.7	0.032 (-0.004-0.067)	3.77E-02
	7	L_Superior-frontal-gyrus	0.06 (0 - 0.212)	0.724	0.027	0.913	2937.5	2937.7	0.029 (-0.006-0.065)	5.37E-02
Rightward	1	R_Parieto-occipital_sulcus	0 (0 - 0.169)	1	0.038	0.962	2939.5	2939.5	**0.06** (0.072-0.142)	**1.63E-04**
	2	R_Inferior-parietal_Lateral-occipital	0.016 (0 - 0.143)	0.927	0.011	0.973	2940.5	2940.5	**0.059** (0.027-0.099)	**4.61E-04**
	3	R_Cingulate	**0.192** (0.077 - 0.309)	**0.016**	0	0.808	2929.8	2935.6	**0.083** (0.011-0.086)	**5.56E-06**
	4	R_Middle-frontal-gyrus	0.025 (0 - 0.139)	0.658	0	0.975	2940.7	2940.9	0.021 (0.151-0.222)	1.24E-01
	5	R_Superior-temporal-sulcus	**0.267** (0 - 0.38)	**0.051**	0	0.733	2918.7	2922.5	**0.078** (0.057-0.13)	**1.02E-05**
	6	R_Superior-frontal-gyrus	0 (0 - 0.118)	1	0.009	0.991	2940.8	2940.8	0.042 (-0.003-0.067)	7.81E-03
	7	R_Gyrus-rectus	0 (0 - 0.132)	1	0.014	0.986	2940.7	2940.7	**0.088** (-0.007-0.066)	**2.09E-07**

***Table 2**: Heritability of asymmetry in clusters exhibiting population-level areal asymmetry. For HCP, heritability was estimated using univariate ACE models with extended twin data (see SI Table 1), whereas for UK Biobank SNP-heritability was estimated (N=31,433). Significant heritability (h^2) estimates are shown in bold (uncorrected for multiple comparisons in HCP and Bonferroni corrected [$p < 3.5e^{-3}$] in UK Biobank). [1]Note the highest SNP-heritability effect was observed for leftward SA asymmetry of the anterior insula cluster (h^2_{SNP} = 18.6%). h^2 = additive genetic effects; c^2 = shared environment effects; e^2 = unique environmental effects + error; -2LL = minus 2 log likelihood index of model fit.*

			HCP (extended twin)						UK Biobank (SNP-based)	
Direction	**ROI #**	**Cluster**	*h2 [± 95% CI]*	*p*	*c2*	*e2*	*-2LL ACE*	*-2LL CE*	*h2 [± 95% CI]*	*p*
Leftward	1	L_Cingulate	0.134 (0 - 0.245)	0.19	0	0.866	2934.6	2936.3	**0.068** (0.032-0.105)	**6.89E-05**
	2	L_Superior-frontal-gyrus	0 (0 - 0.182)	1	0.057	0.943	2937.9	2937.9	0.009 (-0.025-0.044)	2.91E-01
	3	L_Postcentral	0.076 (0 - 0.192)	0.216	0	0.924	2939.1	2940.6	0.024 (-0.012-0.06)	9.88E-02
	4	L_Precentral	0 (0 - 0.084)	1	0.01	0.99	2940.8	2940.8	0.008 (-0.026-0.043)	3.19E-01
	5	L_Supplementary-motor-cortex	0.08 (0 - 0.189)	0.598	0	0.92	2938.6	2938.9	0.012 (-0.023-0.047)	2.59E-01
	6	L_Collateral-sulcus	0 (0 - 0.188)	1	0.053	0.947	2938.2	2938.2	0.034 (-0.002-0.07)	3.38E-02
	7	L_Anterior-transverse-collateral-sulcus	0.095 (0 - 0.21)	0.467	0	0.905	2938.1	2938.6	0.049 (0.013-0.086)	4.38E-03
	8	L_Caudal-middle-frontal	0 (0 - 0.164)	1	0.037	0.963	2939.6	2939.6	0.011 (-0.023-0.046)	2.55E-01
	9	L_Caudal-superior-frontal	0.037 (0 - 0.146)	0.607	0	0.963	2940.4	2940.7	0.024 (-0.011-0.059)	8.16E-02
	10	L_Rostral-superior-frontal	0 (0 - 0.116)	1	0.015	0.985	2940.7	2940.7	0 (-0.033-0.033)	5.00E-01
	11	L_Calcarine-sulcus	0.09 (0 - 0.197)	0.458	0	0.91	2937.9	2938.5	**0.039** (0.003-0.075)	**3.95E-04**
Rightward	1	R_Superior-temporal-sulcus	0.197 (0 - 0.313)	0.257	0.003	0.8	2927.8	2929	0.051 (0.015-0.087)	1.41E-02
	2	R_Lateral-occipital	0 (0 - 0.173)	1	0.062	0.938	2937.1	2937.1	0.019 (-0.015-0.053)	2.67E-03
	3	R_Lingual-gyrus	**0.213** (0.012 - 0.324)	**0.041**	0	0.787	2925.4	2929.6	0.059 (0.024-0.094)	1.30E-01
	4	R_Posterior-insula_Sylvian	0.081 (0 - 0.26)	0.658	0.044	0.875	2933.5	2933.7	**0.033** (-0.001-0.068)	**2.02E-04**
	5	R_Entorhinal	0.032 (0 - 0.138)	0.774	0	0.968	2940.5	2940.6	0.034 (-0.001-0.069)	1.99E-02
	6	R_Superior-insula	0 (0 - 0.126)	1	0.03	0.97	2939.9	2939.9	0.036 (0-0.071)	2.50E-02
	7	R_Planum-temporale	0.035 (0 - 0.145)	0.68	0	0.965	2940.4	2940.6	0 (-0.034-0.034)	2.38E-02
	8	R_Posterior-cingulate	0 (0 - 0.147)	1	0.029	0.971	2939.9	2939.9	0.042 (0.007-0.078)	5.00E-01
	9	R_Anterior-insula	0 (0 - 0.09)	1	0	1	2940.9	2940.9	0.068 (0.032-0.105)	8.95E-03

***Table 3**: Heritability of asymmetry in clusters exhibiting population-level CT asymmetry. For HCP, heritability was estimated using univariate ACE models with extended twin data (see SI Table 1), whereas for UK Biobank SNP-heritability was estimated (N=31,433). Significant heritability (h^2) estimates are shown in bold (uncorrected for multiple comparisons in HCP and Bonferroni corrected [$p < 2.5e^{-3}$] in UK Biobank). h^2 = additive genetic effects; c^2 = shared environment effects; e^2 = unique environmental effects + error; -2LL = minus 2 log likelihood index of model fit.*

Though high heritability estimates were observed for global SA (h^2_{TWIN} = ~.78; h^2_{SNP} = ~.67) and CT (h^2_{TWIN} = ~.75; h^2_{SNP} = ~.36) of each hemisphere (SI Table 6), heritability of global AI measures was low (SA and CT h^2_{TWIN} = ~.03, $p > .7$) and only significant for SA asymmetry in UK Biobank (SA h^2_{SNP} = .06; $p = 2.16e^{-4}$; CT h^2_{SNP} = .01; p = .22). Of our set of population-level asymmetries, only two clusters were estimated to have significantly heritable asymmetry using the HCP twin design and these did not survive multiple comparison correction (see Tables 2-3). In contrast, SNP-based analyses in large-scale data (N=31,433) revealed that 10/14 (72%) of our robust SA asymmetry clusters exhibited significant heritability (including the two with suggestive significance in HCP). Of these, highest heritability was observed for leftward SA in the anterior insula cluster (h^2_{SNP} = 18.6%, $p < 10^{-10}$), which was substantially higher than the next highest estimates which included the large SMG cluster (h^2_{SNP} = 10.7%, $p = 3.01e^{-9}$), retrosplenial cortex, gyrus rectus and the cingulate (all h^2_{SNP} = 8-10%; see Table 2). For CT asymmetry, only 3/20 (15%) clusters exhibited significant SNP-heritability (post Bonferroni correction). These included leftward CT asymmetry in the cingulate (h^2_{SNP} = 6.8%) and calcarine sulcus (h^2_{SNP} = 3.9%), and rightward CT asymmetry in the posterior insula/Sylvian cluster (h^2_{SNP} = 3.3%; see Table 3).

Cortex-wide heritability was then estimated using a fine-grained anatomical parcellation [77] (see Fig. 6). Though again no parcels survived multiple comparison correction in HCP, 53% (267/500) of SA parcels exhibited significant SNP-heritability post FDR-correction in UK Biobank (*p[FDR]*<.05; marked in black outline in Fig. 6A; all parcels with suggestive significance in HCP [also in black outline] survived correction in UK Biobank). Beyond significance, a similar pattern of numerically higher heritability was evident in both samples for SA asymmetry, notably in anterior insula, SMG and the Sylvian fissure, and STS on the lateral side, and around the calcarine sulcus, cingulate, medial and orbitofrontal cortex and fusiform (spatial correlation of maps; r = .38; $p < 10^{-16}$). Importantly, maximum SA SNP-heritability (overlaid in yellow in Fig. 6) was observed in a parcel overlapping the anterior insula SA cluster (parcel h^2_{SNP} = 16.4%; $p < 10^{-10}$), confirming this region constitutes the most heritable cortical asymmetry in humans (and not improving on the cluster-wise estimate). For CT asymmetry, we observed little overlap in heritability estimates between datasets (spatial correlation was significant but low; r = .12; *p* = .01). Significant FDR-corrected SNP-heritability was nevertheless observed around superior temporal gyrus, anterior planum temporale, the posterior insula/Sylvian fissure and in orbitofrontal cortex (max h^2_{SNP} = 16.6%), along the cingulate and in medial visual cortex, though SNP-heritability of CT asymmetry was substantially lower (standardized β = -0.71, $p < 2e^{-16}$), and higher estimates pertained to a few regions that were limited in extent and revealed no clear global SNP-heritability pattern.

For SA, large genetic correlations explained several of the phenotypic correlations observed for opposite-direction asymmetries in Fig. 5A. Fig. 6C shows genetic correlations that survived FDR-correction (78 tests). For example, leftward SA asymmetry in SMG/perisylvian was highly genetically correlated with higher rightward asymmetry in lateral parietal cortex (*rG* = .83; *p(FDR)* = $7.76e^{-05}$), and similarly high genetic correlations were observed for leftward asymmetry in superior frontal cortex and rightward asymmetry along the cingulate (*rG* = .82; *p[FDR]* = $1.36e^{-02}$), and leftward asymmetry in an anterior temporal/parahippocampal cluster and rightward asymmetry in lateral parietal cortex (*rG* = .68; *p[FDR]* = $1.36e^{-02}$). Genetic correlations between leftward asymmetry in anterior insula and rightward asymmetry in two superior frontal gyral clusters were also observed (*rG* = .86; *p[FDR]* = $1.41e^{-06}$; rG = 0.42; *p[FDR]* = $7.74e^{-04}$) in the absence of phenotypic correlations (Fig. 5; SI Fig. 8), and several asymmetries of the same direction showed moderate genetic correlation. For CT, only one cluster-pair survived FDR-correction (49 tests; leftward CT asymmetry of the cingulate and calcarine sulcus; *rG* = 0.68; *p[FDR]* = $3.03e^{-02}$).

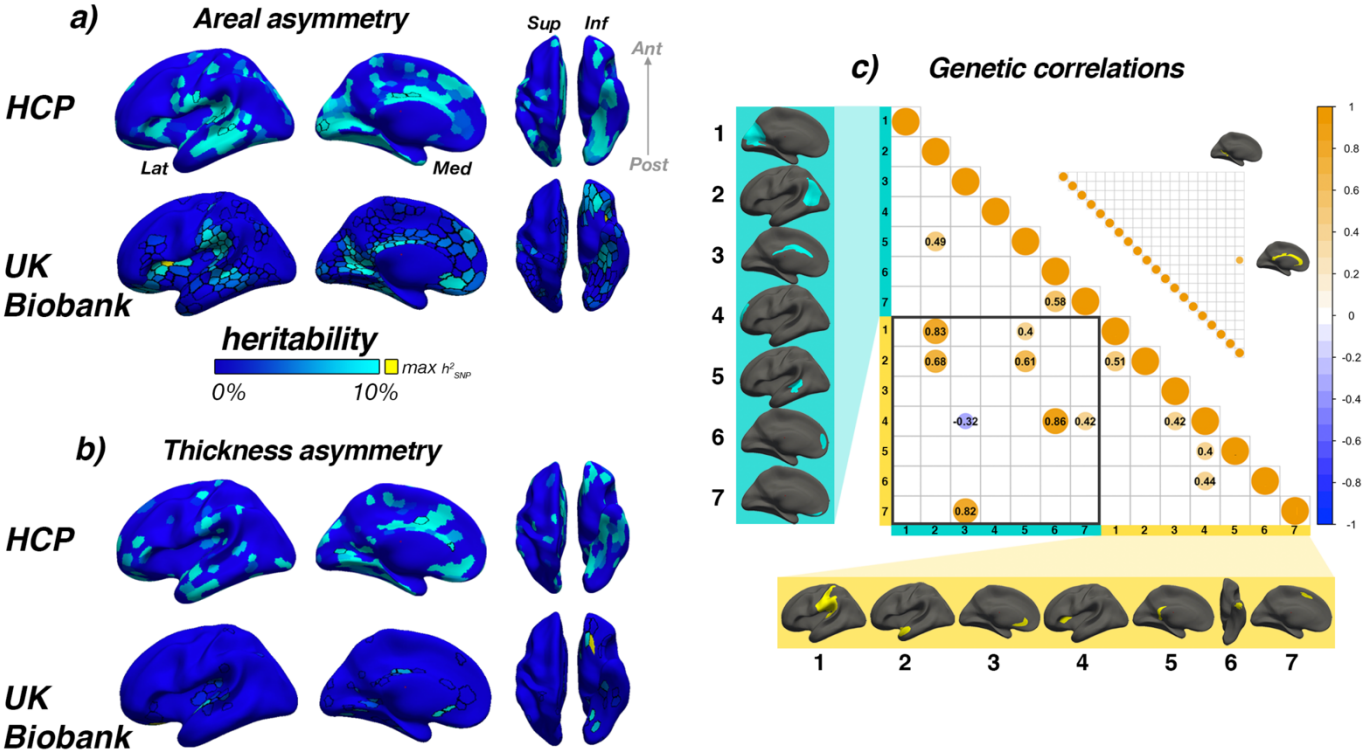

Figure 6. *Heritability estimates of cortical SA* ***(A)*** *and CT asymmetry* ***(B)*** *estimated cortex-wide using a fine-grained anatomical parcellation [77] in HCP (top row) and UK Biobank (bottom). For HCP, heritability was estimated using univariate ACE models with extended twin data (see SI Table 1), whereas for UK Biobank, SNP-heritability was estimated (N=31,433). Unthresholded effect maps are shown (all maps available at neurovault.org/XXXX). In HCP, no parcel survived FDR-correction for multiple comparisons, whereas for UK Biobank, 53.4% of SA (267) and 11.4% of CT (57) parcels survived FDR-correction at p(FDR)<.05. Parcels shown in black outline show significance at p<.05 (uncorrected) for HCP, and at p[FDR]<.05 for UK Biobank (note that all borderline significant parcels in HCP survived correction in UK Biobank). Parcels in yellow depict maximum SNP-heritability for SA (h^2 = 16.4% ± 0.04 CI) and CT (h^2 = 16.6% ± 0.04 CI).* ***C)*** *Pairwise genetic correlations in clusters exhibiting population-level SA (lower matrix) and CT asymmetry (upper matrix) estimated in UK Biobank (N=31,433). Yellow and blue brain clusters/colours denote population-level leftward and rightward asymmetries,*

respectively (clusters numbered for reference). For SA, large genetic correlations explained several observed phenotypic correlations in Fig. 5A. For CT, only one cluster-pair exhibited FDR-corrected significance (shown). Pair-wise genetic correlations were tested only for clusters exhibiting significant heritability at p < .05 [uncorrected] (78 tests for SA; 49 for CT). AI's in rightward clusters were inversed such that positive genetic correlations denote positive asymmetry-asymmetry genetic relationships regardless of direction.

3.5 Associations with Cognition, Handedness, Sex, and ICV

Several significant effects (post-correction) were observed for associations between factors-of-interest and asymmetry in our robust SA and CT asymmetry clusters (Fig. 7). Notably, all effect sizes were small. For general cognitive ability, we found one association: higher SA asymmetry in the largest leftward cluster (SMG/perisylvian) was significantly associated with better cognition (standardized β =.03 [CI = 0.02 – 0.04], p = 4.1e^{-7}). This effect was checked in the substantially reduced non-imputed subset of data with no missing cognitive variables (N = 4696; β =0.04 [CI = 0.01 - 0.07]; p = 6.9e^{-3}) and retained the lowest p-value of all tested associations with cognition. For handedness, reduced leftward SA asymmetry in anterior insula and CT asymmetry along postcentral gyrus was found in left-handers, in line with our recent vertex-wise mapping in UK Biobank [29]. For sex effects, which were also small, males typically exhibited slightly stronger SA asymmetry in large clusters (e.g. leftward SMG/perisylvian and temporal pole; rightward inferior parietal and superior frontal) but reduced leftward and rightward asymmetry in mPFC. For CT, males exhibited more rightward asymmetry in a large cluster encompassing STS and in posterior insula, stronger leftward CT asymmetry in superior frontal cortex, but reduced rightward CT asymmetry in entorhinal cortex and anterior insula, and reduced leftward asymmetry in caudal superior frontal cortex. As effects of ICV were the most nominal, these are described in SI Fig. 11 (stats in SI Tables 7-10).

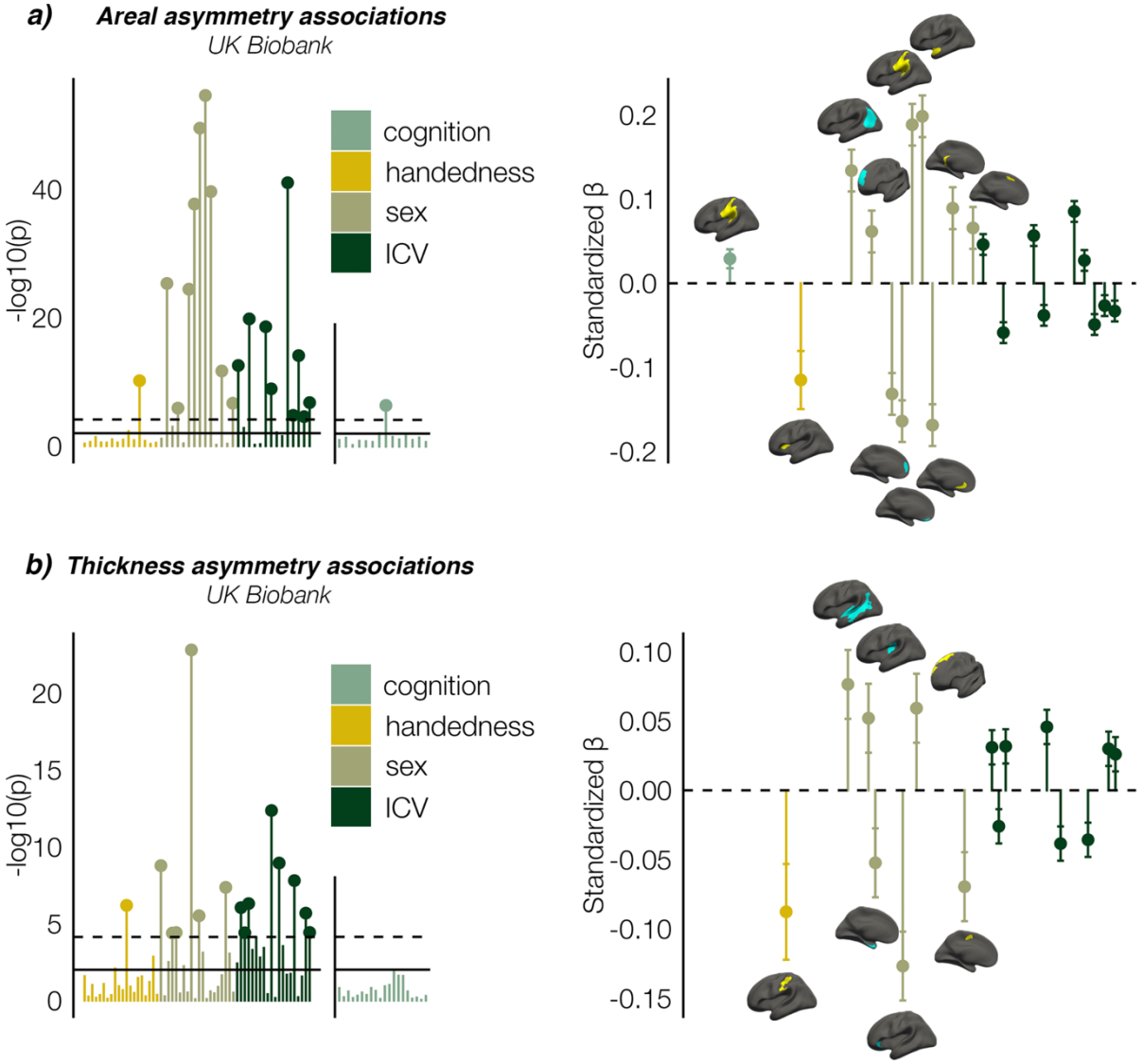

Figure 7. *Asymmetry associations with general cognitive ability (first principal component), Handedness, Sex, and estimated intracranial volume (ICV) in UK Biobank, in clusters exhibiting population-level* ***A)*** *SA and* ***B)*** *CT asymmetry. Left plots denote significance of associations (negative logarithm; Bonferroni corrected [p < 7.3e^{-5}] and uncorrected*

threshold [p = .01] given by horizontal dotted and non-dotted line, respectively). X-axis displays the test for each cluster-association. As the maximum sample size was used to test each association (Handedness, Sex and ICV: N=37,570), effects on cognition were tested in separate models with fewer observations (N = 35,199) and are thus shown on separated association plots. Right plots denote the effect sizes (standardized Betas), 95% confidence intervals (error bars) and cortical location of all associations surpassing Bonferroni-corrected significance. Right handers and females are coded 0, such that a negative effect size for handedness / sex / ICV / cognition denotes less asymmetry in left handers / males / larger brains / higher cognition. Associations with ICV were typically the most nominal and for visualization purposes are shown in SI Fig. 11 (see also SI Tables 7-9). Blue and yellow clusters denote leftward and rightward asymmetries, respectively.

4. Discussion

We provide a reference for population-level cortical asymmetries using 7 international datasets and offer the first description of the longitudinal lifespan trajectories of cortical asymmetry. Our results demonstrate the replicable interregional relationships between asymmetries within individuals, provide the most detailed heritability maps for cortical asymmetry to date, uncover novel and confirm previously-reported associations with factors reportedly related to asymmetry in large-scale data, and further knowledge on normal brain development. All maps are available at neurovault.org/XXXX.

Our vertex-wise description of cortical asymmetries that reproduce across multiple cohorts replicates and completes a recent low-resolution meta-analysis [8], and can serve as a high-fidelity phenotype for future brain asymmetry studies. The marked consistency across samples here suggests consensus may now be reached regarding cortical asymmetry phenotypes in humans, as these results agree with most of the literature [8,9,15,20,25,31,33], including a recent large-scale mapping in mid-old age [29]. This consensus, along with the genetic findings presented herein, suggests genetic-developmental programs regulate mean brain lateralization with respect to SA, and the trajectories observed here suggest this form of cerebral asymmetry is maintained throughout life and formed early on – likely *in utero* [31,39]. For CT asymmetry – for which findings have been particularly mixed [8,9,11–21] – the left-right patterning observed here is compatible with recent reports [11,29], studies examining CT asymmetry from birth [12], global meta-analyses [8], reports using alternative analysis streams [12,21], anatomical asymmetries evident early in ontogeny [88–91], and leftward CT asymmetry overlapping language- [92] and motor-related regions [15,93–95]. This consistency across adult samples may also indicate that mean CT asymmetry is genetically regulated at the population-level in humans. However, our findings of development and decline of CT asymmetry across life [11], higher directional variability in adult samples and lower heritability also converge to suggest CT asymmetry may be more prone to lifespan change, potentially more malleable to life experience, and susceptible to lifespan accumulation of insult. Though it remains possible CT asymmetry change could be genetically-regulated into old age, this interpretation agrees with work suggesting SA may trace to prenatal factors [96,97] whereas CT relates more to postnatal lifespan influences [97,98].

Our results suggest conceivable sources of previously inconsistent results may be the age-distribution under study [11] and the existence of varying directional asymmetries within the population (for CT asymmetry). This may partly explain why metrics of CT asymmetry are more variable across datasets compared with SA [8], though CT asymmetry effects are also smaller [9,15,20] and likely contain more measurement error. Varying directional asymmetry within atlas-based parcels may also explain inconsistent reports, such as in insular cortex where we observed consistent but discrepant asymmetry to that reported in ENIGMA [8]. However, this does not account for the discrepancy that studies using the same atlas [26] typically report areal asymmetry in STS to be left-lateralized [8,32,33], as the right-lateralization evidenced here and elsewhere [15,31] seems unambiguous. Of note, although we did not find strong SA asymmetry in inferior frontal regions as reported by Kong et al [8], the unthresholded significance maps were somewhat compatible with this (SI Fig. 3). The high overlap in effects between 7 datasets from 4 countries suggests our results apply universally, though future studies will be needed to confirm this in non-American/North European samples.

Our longitudinal description of the lifespan trajectories of cortical asymmetry gleaned novel insight into the normal development of brain asymmetries. For SA asymmetry, adult-patterns of lateralization were strongly established already before ~4 years, indicating SA asymmetry traces back further and does not primarily emerge through later cortical expansion [99,100]. Rather, the lifespan trajectories of SA asymmetry predominantly show stability from childhood to old age, as asymmetry was generally maintained through periods of developmental expansion and aging-associated change that were region-specific and bilateral. This agrees with evidence indicating SA asymmetry is primarily determined *in utero* [31], and indirect evidence suggesting little change in SA asymmetry from birth to 2 years despite rapid and concurrent [31,35] developmental expansion of the cortex [99,100]. It may also fit with the principle that the primary microstructural basis of SA [37] – the number

of and spacing between cortical minicolumns – is determined in prenatal life [37,38,98]. Indeed, some evidence suggests asymmetry at this microstructural level may underly regional hemispheric differences in SA [36,101,102], which may fit with the lifelong maintenance of SA asymmetry we observed. The developmental trajectories agree with longitudinal [31] and cross-sectional studies [33] indicating SA asymmetry is established [31] and strongly directional early in life [33]. That anatomical change in later development specifically in SA follows embryonic gene expression gradients may also agree with a prenatal account for SA asymmetry [98]. These results may therefore constrain the extent to which SA asymmetry can be viewed as a plastic feature of brain organization, and may even suggest SA asymmetry may sometimes be a marker for innate hemispheric specializations shared by most humans. The high degree of precision with which leftward SA asymmetry follows the contours of auditory-related regions in the Sylvian fissure (SI Fig. 1A) which show left functional lateralization in humans may be one example supported by recent research [36,103,104].

In stark contrast, although weak CT asymmetry was evident by age 4, we observed considerable developmental growth and lifespan change in CT asymmetry thereafter. Developmental trajectories showed non-linear asymmetry growth by virtue of accelerated thinning of the non-dominant hemisphere, and led to a maximally established asymmetry around ~25 years of age. These trajectories clearly suggest differentiation of the cortex is occurring with respect to CT asymmetry in development, possibly suggesting CT asymmetry may be more amenable to experience-dependent plastic change. Indeed, cortical thinning in childhood is thought to partly reflect likely learning-dependent processes such as intracortical myelination [105] and possibly pruning of initially overproduced synapses [106–108] and reductions in neuropil. CT asymmetry may thus reflect hemispheric differences in the developmental optimization of cortical networks at least partly shaped by childhood experience. This raises the possibility CT asymmetry may be a marker of ontogenetic hemispheric specialization within neurocognitive networks. Our findings in development agree with work finding a similar left-right patterning of CT asymmetry shows rapid asymmetry increase in the first years of life [12], with especially rapid increase in leftward mPFC [12]. As we also observed rapid differentiation in mPFC that spanned across childhood and adolescence (Fig 4A; SI Figs. 5-6), we extend these earlier findings in neonates [12]. As prefrontal CT asymmetry seems particularly vulnerable in neurodevelopmental disorders [22], aging, and Alzheimer's disease [11], these trajectories may provide a useful normative reference. With regards to aging, most clusters exhibited the expected aging-associated reduction of CT asymmetry we have previously shown is a feature of aging in heteromodal cortex [11]. This differentiation and dedifferentiation of CT asymmetry at either end of life underscores its proposed role in supporting optimal brain organization and function [11].

For SA asymmetry, we uncovered a covariance structure that almost perfectly replicated across datasets. In general, this fit with a multifaceted nature of brain asymmetry [32,43,44], in which most asymmetries were either not or only weakly correlated, but reliably so. Importantly, however, we identified several regions wherein SA asymmetry reliably correlated within individuals, showing the variance in structural cortical asymmetries is not always dissociable, as is often thought [32,43,109]. The strongest relationships all pertained to asymmetries that were proximal in the cortex but opposite in direction (i.e. leftward asymmetry in left-asymmetric regions related to more rightward asymmetry in right-asymmetric regions). Several of these were underpinned by high positive asymmetry-asymmetry genetic correlations, illustrating cerebral lateralizations in SA that are formed under common genetic-developmental influence, and in agreement with likely prenatal origins for SA asymmetry [31,38].

For CT asymmetry, we also uncovered a common covariance structure – particularly clear in UK Biobank – that nevertheless replicated with moderate precision across datasets. Furthermore, a single global factor explained a relatively high proportion of the variance in CT asymmetry in UK Biobank, and a strong correlation across 38,172 individuals further suggested CT asymmetry is globally interrelated across the cortex (Fig. 5D; SI Fig. 10). These data for CT indicate individuals tend towards either leftward asymmetry, rightward asymmetry, or symmetry, both globally across the cortex and irrespective of the region-specific average direction of asymmetry (SI Fig. 8-9). This result seems in broad agreement with the notion that some lateralized genetic-developmental programs may trigger lateralization in either direction [44] or lose their directional bias through interaction with the environment [44]. As CT asymmetry seems established at but minimal from birth [12], genetic effects may determine the average region-specific hemispheric bias in the population, but high developmental change may subsequently confer major increases upon its directional variance [44]. Overall, the evidence converges to suggest a high degree of developmental change may shape CT asymmetry and lead to higher directional variability in the population. Thus, far from being independent phenotypes [32,43], CT asymmetries may be globally interrelated across the cortex and their direction coordinated through development.

For SA asymmetry, cortex-wide heritability mapping revealed replicable patterns of moderate heritability across datasets and across twin-based and genomic methods. We also found SA asymmetry in the anterior insula is

to our knowledge the most heritable asymmetry yet reported with genomic methods [29,39,110], with common SNPs explaining ~19% of its variance. This is a substantial improvement on our recent report of < 5% [29], and illustrates a benefit of our data-driven population-mapping approach. Interestingly, as we reported recently [29], we confirm asymmetry in this region associates with handedness (see below). Furthermore, highest SNP-heritability for SA was found in all regions that constitute the earliest developing cortical asymmetries *in utero* [88,111–113]: anterior insula, STS, PT, medial occipital cortex, and parahippocampal gyrus (Fig. 6A). Still, results extended beyond these, as most SA asymmetries exhibited significant – albeit often lower – heritability, as did most parcels when estimated cortex-wide. Significant SNP-heritability was also observed in regions not found to show strong SA asymmetry, such as Broca's area. The regional effects agree with and elaborate on two previous genetic explorations using atlas-based methods [8,39] and reports of significantly heritable SA asymmetry in handedness-associated clusters [29]. By contrast, CT asymmetry was generally not heritable, or showed low and localized heritability effects. We also observed divergent results using twin-based and genomic methods for CT, possibly in part due to low-power for twin-models, though we note the SNP-based effects we observed were somewhat in agreement with a previous twin-based study of cortical asymmetry heritability [8]. Overall, these reproducible results may guide phenotypic selection in future genomic and biological studies on cerebral laterality.

Considered together, lifespan stability possibly from birth [31], less interindividual directional variability, higher heritability, and phenotypic and genetic correlations all converge to suggest comparatively higher genetic influence upon SA asymmetry and possibly limited plasticity. This agrees with work showing genetic variants associated with (mostly SA) asymmetry are primarily expressed in prenatal life [39]. By contrast, developmental change, high interindividual directional variability and low heritability for CT asymmetry may fit a scenario whereby CT asymmetry may be more responsive to postnatal individual exposures [98], or driven by random developmental influences [114]. Whether region-specific CT asymmetry-change relates to the maturation of lateralized brain functions [114,115] will be an important question for future research. Regardless, our results support a relative prenatal-postnatal developmental dichotomy for SA and CT asymmetry.

Screening population-level asymmetries for association with cognitive ability revealed one region – SMG/perisylvian – wherein higher leftward asymmetry relates to higher cognition. Across all samples tested this cluster was consistently the most lateralized, showing a ~95% concordance rate in direction (SI Fig. 2), suggesting highly regulated genetic-developmental programs shape its laterality in humans. Asymmetry in this region is likely related to brain torque [30,50,116], a gross anatomical twist of the hemispheres leading to inter-hemispheric anatomical differences especially around the Sylvian fissure [30]. Given that brain torque also represents a population-level directional norm in humans [117], this result suggests disruptions in prenatal cerebral lateralization may lead to cognitive deficits detectable in later life, and agrees with recent work suggesting brain torque may be related to cognitive outcome variables [51,117]. That this was found specifically in the most lateralized SA cluster may agree with work suggesting general cognitive abilities that are intra-individually stable across life [118–121] relate primarily to SA phenotypes that depend mostly on prenatal factors [96,98].

Consistent with our recent vertex-wise analysis in UK Biobank [29], we confirmed leftward SA asymmetry of the anterior insula, and leftward CT asymmetry of somatosensory cortex, is subtly reduced in left handers. Sha et al. [29] reported shared genetic influences upon handedness and cortical asymmetry in anterior insula and other more focal regions not identified with the approach used here. Anterior insula lies within a left-lateralized functional language network [122], and its structural asymmetry may relate to language lateralization [42,123–125]. Speculatively, reduced anterior insula SA asymmetry in left handers may be related to increased incidence of atypical language lateralization in this group [55,126–129]. Together with observations that anterior insula asymmetry emerges early *in utero* [111,130], we agree with others [42] that future research will find this ontogenetically foundational region of cortex [131,132] a fruitful line of inquiry for understanding genetic-developmental mechanisms influencing diverse laterality phenotypes.

The observed leftward CT asymmetry reduction in somatosensory cortex in left handers also echoes our recent report, where it was suggested to reflect plastic adaptation to an already-established hand preference [29]. We extend these results by showing CT asymmetry both postcentrally and in general shows developmental differentiation and lifespan change. Given that this cluster overlaps with functional representations of the hands [93,94,133] – as in Sha et al. [29] – and our improved mapping approach also detected no significant heritability, these findings may fit a scenario whereby CT asymmetries are amenable to alteration through use-dependent plasticity and may carry information regarding group-level hemispheric specializations of function. However, the small effects cast doubt on the utility of cortical asymmetry measures to accurately predict individual hand preference.

Asymmetry-relationships with other factors were often compatible with those reported in the ENIGMA meta-analysis [8]. Concerning sex effects – which were small and differing in direction – we similarly observed leftward SA asymmetry in temporal and SMG/perisylvian regions to be larger in males [8], replicating earlier findings [41]. Previous genetic analyses imply steroid-hormone pathways underly this difference [41], and sex in general was found to be more predictive than ICV both here and elsewhere [41]. We also found lower SA asymmetry in comparable regions of medial prefrontal cortex in males compatible with this earlier report [8]. Inconsistencies evident between ours and the ENIGMA report include findings of increased (here) and decreased [8] lateral parietal SA asymmetry in males, and increased [8] and decreased (here) entorhinal CT asymmetry in males, and our approach detected other regions slightly more asymmetric in males (e.g. STS). Possibly, differences in sample median age (here UK Biobank = ~64; Kong et al. = 26 [8]) and potential sex-differences in age decline trajectories [134] may underlie some inconsistencies, possibly moreso for CT measures in structures vulnerable to age-related degeneration [11,87,135].

Several limitations should be mentioned. First, our delineation of population-level asymmetry used a single analysis software, and it is unclear to what extent differences in pipelines account for mixed results [8,9,11–21], though several studies suggest our results reproduce across analysis systems [12,13,21,25]. Second, while GAMMs are considered an optimal modelling technique for longitudinal lifespan data and are robust to non-normal age distributions [73], relative underrepresentation of the mid-adulthood age-range may drive trajectory inflection points around this age [11], suggesting caution is warranted regarding interpreting mid-life inflection points as reflecting real change. Third, though the differing heritability methods applied enabled replication for SA, twin studies are prone to overestimating heritability due to unmet assumptions [79,81], whereas SNP-based methods may not capture all phenotype-relevant genetic variance, and have their own assumptions [136,137]. Indeed, we found twin-based estimates were often substantially higher even where only nominally significant, agreeing with recent calls for caution when interpreting twin-based heritability estimates [81]. Fourth, we imposed a necessary cluster size limit for overlapping asymmetry effects across samples, and thus more focal asymmetries may also be informative in relation to the factors tested here (see [29]). Fifth, as only dichotomous handedness self-reports are available with UK Biobank, future studies might benefit from incorporating more nuanced handedness assessments not currently available in data of this size [126,128]. Relatedly, because UK Biobank cognitive data is not exhaustive (e.g. fluid IQ ranges from 1-13) [84], we extracted the common variance across core tests to index general cognitive ability. This approach did not permit testing associations with specific cognitive abilities, which may be highly informative in the context of asymmetry, particularly in the case of lateralized cognition [101,138,139].

Overall, we provide an openly-available comprehensive characterization of asymmetry in the cerebral cortex including longitudinal lifespan changes, heritability, and individual differences that bears enough reproducibility to be used as a standard in future research.

Data sharing/availability

All summary-level maps are available at neurovault.org/XXXX (upon acceptance), and maps, shareable data and code are available at https://github.com/jamesmroe/PopAsym. All datasets used in this work are openly available, with the exception of LCBC, where participants have not consented to publicly share data. DLBS, SALD, and IXI are available without restrictions under Creative Commons Licenses (https://fcon_1000.projects.nitrc.org/indi/retro/dlbs.html; CC BY-NC; http://fcon_1000.projects.nitrc.org/indi/retro/sald.html; CC BY-NC; https://brain-development.org/ixi-dataset; CC BY-SA 3.0). Accordingly, we have made the individual-level maps for these samples available and our code can be used to reproduce vertex-wise analyses in these samples. As differing restrictions apply to the remaining samples (Cam-CAN, HCP; UK Biobank), requests for data access must be submitted and approved via the relevant channel.

Acknowledgements

Scripts were ran on the Colossus processing cluster at the University of Oslo, and on resources provided by UNINETT Sigma2 - the National Infrastructure for High Performance Computing and Data Storage in Norway (project NN9769K). LCBC funding: European Research Council under grant agreements 283634, 725025 (to A.M.F.), and 313440 (to K.B.W.); Norwegian Research Council (to A.M.F. and K.B.W.) under grant agreements 249931 (TOPPFORSK) and 302854 (FRIPRO; to Y.W.), The National Association for Public Health's dementia research program, Norway (to A.M.F). Some of the data used in the preparation of this work were obtained

from the MGH-USC Human Connectome Project (HCP) database (https://ida.loni.usc.edu/login.jsp). The HCP project (Principal Investigators: Bruce Rosen, M.D., Ph.D., Martinos Center at Massachusetts General Hospital; Arthur W. Toga, Ph.D., University of Southern California, Van J. Weeden, MD, Martinos Center at Massachusetts General Hospital) is supported by the National Institute of Dental and Craniofacial Research (NIDCR), the National Institute of Mental Health (NIMH) and the National Institute of Neurological Disorders and Stroke (NINDS).

4.9 References

1. van Kesteren, E.-J. & Kievit, R. A. Exploratory factor analysis with structured residuals for brain network data. *Netw. Neurosci.* 1–45 (2020). doi:10.1162/netn_a_00162
2. Stark, D. E. *et al.* Regional Variation in Interhemispheric Coordination of Intrinsic Hemodynamic Fluctuations. *J. Neurosci.* **28**, 13754–13764 (2008).
3. Schmitt, J. E., Giedd, J. N., Raznahan, A. & Neale, M. C. The genetic contributions to maturational coupling in the human cerebrum: A longitudinal pediatric twin imaging study. *Cereb. Cortex* **28**, 3184–3191 (2018).
4. Chen, C. H. *et al.* Genetic topography of brain morphology. *Proc. Natl. Acad. Sci. U. S. A.* **110**, 17089–17094 (2013).
5. Chen, C. H. *et al.* Hierarchical genetic organization of human cortical surface area. *Science (80-.).* **335**, 1634–1636 (2012).
6. Eyler, L. T. *et al.* Conceptual and Data-based Investigation of Genetic Influences and Brain Asymmetry: A Twin Study of Multiple Structural Phenotypes. *J. Cogn. Neurosci.* **26**, 1100–1117 (2014).
7. Raznahan, A. *et al.* Patterns of coordinated anatomical change in human cortical development: A longitudinal neuroimaging study of maturational coupling. *Neuron* **72**, 873–884 (2011).
8. Kong, X.-Z. *et al.* Mapping cortical brain asymmetry in 17,141 healthy individuals worldwide via the ENIGMA Consortium. *Proc. Natl. Acad. Sci.* **115**, E5154–E5163 (2018).
9. Chiarello, C., Vazquez, D., Felton, A. & McDowell, A. Structural asymmetry of the human cerebral cortex: Regional and between-subject variability of surface area, cortical thickness, and local gyrification. *Neuropsychologia* **93**, 365–379 (2016).
10. Meyer, M., Liem, F., Hirsiger, S., Jäncke, L. & Hänggi, J. Cortical surface area and cortical thickness demonstrate differential structural asymmetry in auditory-related areas of the human cortex. *Cereb. Cortex* **24**, 2541–2552 (2014).
11. Roe, J. M. *et al.* Asymmetric thinning of the cerebral cortex across the adult lifespan is accelerated in Alzheimer's disease. *Nat. Commun.* **12**, 1–11 (2021).
12. Li, G., Lin, W., Gilmore, J. H. & Shen, D. Spatial patterns, longitudinal development, and hemispheric asymmetries of cortical thickness in infants from birth to 2 years of age. *J. Neurosci.* **35**, 9150–9162 (2015).
13. Luders, E. *et al.* Hemispheric asymmetries in cortical thickness. *Cereb. Cortex* **16**, 1232–1238 (2006).
14. Zhou, D., Lebel, C., Evans, A. & Beaulieu, C. Cortical thickness asymmetry from childhood to older adulthood. *Neuroimage* **83**, 66–74 (2013).
15. Maingault, S., Tzourio-Mazoyer, N., Mazoyer, B. & Crivello, F. Regional correlations between cortical thickness and surface area asymmetries: A surface-based morphometry study of 250 adults. *Neuropsychologia* **93**, 350–364 (2015).
16. Shaw, P., Lalonde, F. & Al, L. C. et. Development of Cortical Asymmetry in Typically Developing Children and Its Disruption in Attention-Deficit/Hyperactivity Disorder. **66**, 888–896 (2009).
17. Lou, Y. *et al.* Brain asymmetry differences between Chinese and Caucasian populations : a surface-based morphometric comparison study. (2019).
18. Hamilton, L. S. *et al.* Asymmetries of cortical thickness: Effects of handedness, sex, and schizophrenia. *Neuroreport* **18**, 1427–1431 (2007).
19. Zhou, D. *et al.* Preserved cortical asymmetry despite thinner cortex in children and adolescents with prenatal alcohol exposure and associated conditions. *Hum. Brain Mapp.* **39**, 72–88 (2018).
20. Koelkebeck, K. *et al.* The contribution of cortical thickness and surface area to gray matter asymmetries in the healthy human brain. *Hum. Brain Mapp.* **35**, 6011–6022 (2014).
21. Plessen, K. J., Hugdahl, K., Bansal, R., Hao, X. & Peterson, B. S. Sex, age, and cognitive correlates of asymmetries in thickness of the cortical mantle across the life span. *J Neurosci* **34**, 6294–6302 (2014).
22. Postema, M. C. *et al.* Altered structural brain asymmetry in autism spectrum disorder in a study of 54 datasets. *Nat. Commun.* **10**, 1–12 (2019).
23. Thompson, P. M. *et al.* Tracking Alzheimer's disease. *Ann. N. Y. Acad. Sci.* **1097**, 183–214 (2007).
24. Long, X., Jiang, C. & Zhang, L. Morphological biomarker differentiating MCI converters from nonconverters: Longitudinal evidence based on hemispheric asymmetry. *Behav. Neurol.* **2018**, (2018).
25. Lyttelton, O. C. *et al.* Positional and surface area asymmetry of the human cerebral cortex. *Neuroimage* **46**, 895–903 (2009).
26. Desikan, R. S. *et al.* An automated labeling system for subdividing the human cerebral cortex on MRI scans into gyral based regions of interest. *Neuroimage* **31**, 968–80 (2006).
27. Destrieux, C., Fischl, B., Dale, A. & Halgren, E. Automatic parcellation of human cortical gyri and sulci using standard anatomical nomenclature. *Neuroimage* **53**, 1–15 (2010).
28. Roe, J. M. *et al.* Age-Related Differences in Functional Asymmetry during Memory Retrieval Revisited: No Evidence for Contralateral Overactivation or Compensation. *Cereb. Cortex* **30**, 1129–1147 (2020).
29. Sha, Z. *et al.* Handedness and its genetic influences are associated with structural asymmetries of the cerebral cortex in 31,864 individuals. *Proc. Natl. Acad. Sci.* **118**, 1–9 (2021).
30. Toga, a W. & Thompson, P. M. Mapping brain asymmetry. *Nat. Rev. Neurosci.* **4**, 37–48 (2003).
31. Li, G. *et al.* Mapping longitudinal hemispheric structural asymmetries of the human cerebral cortex from birth to 2 years

of age. *Cereb. Cortex* **24**, 1289–1300 (2014).
32. Bain, J. S., Filo, S. & Mezer, A. A. The robust and independent nature of structural STS asymmetries. *Brain Struct. Funct.* **224**, 3171–3182 (2019).
33. Remer, J. *et al.* Quantifying cortical development in typically developing toddlers and young children, 1–6 years of age. *Neuroimage* **153**, 246–261 (2017).
34. Nie, J., Li, G. & Shen, D. Development of cortical anatomical properties from early childhood to early adulthood. *Neuroimage* **76**, 216–224 (2013).
35. Li, G. *et al.* Mapping region-specific longitudinal cortical surface expansion from birth to 2 years of age. *Cereb. Cortex* **23**, 2724–2733 (2013).
36. Chance, S. A., Casanova, M. F., Switala, A. E. & Crow, T. J. Minicolumnar structure in Heschl's gyrus and planum temporale: Asymmetries in relation to sex and callosal fiber number. *Neuroscience* **143**, 1041–1050 (2006).
37. Rakic, P. A small step for the cell, a giant leap for mankind: a hypothesis of neocortical expansion during evolution. *Trends Neurosci.* **18**, 383–388 (1995).
38. Rakic, P. The radial edifice of cortical architecture: From neuronal silhouettes to genetic engineering. *Brain Res. Rev.* **55**, 204–219 (2007).
39. Sha, Z. *et al.* The genetic architecture of structural left–right asymmetry of the human brain. *Nat. Hum. Behav.* (2021). doi:10.1038/s41562-021-01069-w
40. Tadayon, S. H., Vaziri-Pashkam, M., Kahali, P., Dezfouli, M. A. & Abbassian, A. Common genetic variant in VIT is associated with human brain asymmetry. *Front. Hum. Neurosci.* **10**, 1–8 (2016).
41. Guadalupe, T. *et al.* Asymmetry within and around the human planum temporale is sexually dimorphic and influenced by genes involved in steroid hormone receptor activity. *Cortex* **62**, 41–55 (2015).
42. Chiarello, C., Vazquez, D., Felton, A. & Leonard, C. M. Structural asymmetry of anterior insula: Behavioral correlates and individual differences. *Brain Lang.* **126**, 109–122 (2013).
43. Rentería, M. E. Cerebral asymmetry: A quantitative, multifactorial, and plastic brain phenotype. *Twin Res. Hum. Genet.* **15**, 401–413 (2012).
44. Francks, C. Exploring human brain lateralization with molecular genetics and genomics. *Ann. N. Y. Acad. Sci.* **1359**, 1–13 (2015).
45. Liu, H., Stufflebeam, S. M., Sepulcre, J., Hedden, T. & Buckner, R. L. Evidence from intrinsic activity that asymmetry of the human brain is controlled by multiple factors. *Proc. Natl. Acad. Sci. U. S. A.* **106**, 20499–20503 (2009).
46. Crow, T. J., Crow, L. R., Done, D. J. & Leask, S. Relative hand skill predicts academic ability: Global deficits at the point of hemispheric indecision. *Neuropsychologia* **36**, 1275–1282 (1998).
47. Ocklenburg, S., Güntürkün, O., Hugdahl, K. & Hirnstein, M. Laterality and mental disorders in the postgenomic age – A closer look at schizophrenia and language lateralization. *Neurosci. Biobehav. Rev.* **59**, 100–110 (2015).
48. Zickert, N., Geuze, R. H., Beking, T. & Groothuis, T. G. G. Testing the Darwinian function of lateralization. Does separation of workload between brain hemispheres increase cognitive performance? *Neuropsychologia* **159**, 107884 (2021).
49. Kong, X.-Z. *et al.* Large-Scale Phenomic and Genomic Analysis of Brain Asymmetrical Skew. *Cereb. Cortex* 1–18 (2021). doi:10.1093/cercor/bhab075
50. LeMay, M. Morphological Cerebral Asymmetries of Modern Man, Fossil Man, and Nonhuman Primate. *Ann. N. Y. Acad. Sci.* **280**, 349–366 (1976).
51. Zhao, L., Matloff, W., Shi, Y., Cabeen, R. P. & Toga, A. W. Mapping Complex Brain Torque Components and Their Genetic and Phenomic Architecture in 24 , 112 healthy individuals. (2021).
52. Moodie, J. E. *et al.* Fluctuating asymmetry in brain structure and general intelligence in 73-year-olds. *Intelligence* **78**, 101407 (2020).
53. Yeo, R. A., Ryman, S. G., Pommy, J., Thoma, R. J. & Jung, R. E. General cognitive ability and fluctuating asymmetry of brain surface area. *Intelligence* **56**, 93–98 (2016).
54. Kong, X. *et al.* Mapping brain asymmetry in health and disease through the ENIGMA consortium. *Hum. Brain Mapp.* 1–15 (2020).
55. Wiberg, A. *et al.* Handedness , language areas and neuropsychiatric diseases : insights from brain imaging and genetics. *Brain* 1–10 (2019). doi:10.1093/brain/awz257
56. Eyler, L. T. *et al.* A comparison of heritability maps of cortical surface area and thickness and the influence of adjustment for whole brain measures: A magnetic resonance imaging twin study. *Twin Res. Hum. Genet.* **15**, 304–314 (2012).
57. van der Meer, D. *et al.* Quantifying the Polygenic Architecture of the Human Cerebral Cortex: Extensive Genetic Overlap between Cortical Thickness and Surface Area. *Cereb. Cortex* **30**, 5597–5603 (2020).
58. Miller, K. L. *et al.* Multimodal population brain imaging in the UK Biobank prospective epidemiological study. *Nat. Neurosci.* **19**, 1523–1536 (2016).
59. Shafto, M. A. *et al.* The Cambridge Centre for Ageing and Neuroscience (Cam-CAN) study protocol: A cross-sectional, lifespan, multidisciplinary examination of healthy cognitive ageing. *BMC Neurol.* **14**, 1–25 (2014).
60. Taylor, J. R. *et al.* The Cambridge Centre for Ageing and Neuroscience (Cam-CAN) data repository: Structural and functional MRI, MEG, and cognitive data from a cross-sectional adult lifespan sample. *Neuroimage* **144**, 262–269 (2017).
61. Kennedy, K. M. *et al.* Effects of beta-amyloid accumulation on neural function during encoding across the adult lifespan. *Neuroimage* **62**, 1–8 (2012).
62. Wei, D. *et al.* Data Descriptor: Structural and functional brain scans from the cross-sectional Southwest University adult lifespan dataset. *Sci. Data* **5**, 1–10 (2018).
63. Van Essen, D. C. *et al.* The WU-Minn Human Connectome Project: An overview. *Neuroimage* **80**, 62–79 (2013).
64. Fjell, A. M. *et al.* Self-reported sleep relates to hippocampal atrophy across the adult lifespan - results from the Lifebrain consortium. *Sleep* 1–15 (2019). doi:10.1093/sleep/zsz280
65. Vidal-Pineiro, D. *et al.* Cellular correlates of cortical thinning throughout the lifespan. Preprint at https://www.biorxiv.org/content/10.1101/585786v3. (2019).
66. Fischl, B. & Dale, A. M. Measuring the thickness of the human cerebral cortex from magnetic resonance images. *Proc. Natl. Acad. Sci. U. S. A.* **97**, 11050–5 (2000).
67. Fischl, B. *et al.* Sequence-independent segmentation of magnetic resonance images. *Neuroimage* **23 Suppl 1**, S69-84 (2004).
68. Reuter, M., Rosas, H. D. & Fischl, B. Highly accurate inverse consistent registration: a robust approach. *Neuroimage*

53, 1181–96 (2010).
69. Marie, D., Maingault, S., Crivello, F., Mazoyer, B. & Tzourio-Mazoyer, N. Surface-Based Morphometry of Cortical Thickness and Surface Area Associated with Heschl's Gyri Duplications in 430 Healthy Volunteers. *Front. Hum. Neurosci.* **10**, (2016).
70. Greve, D. *et al.* A Surface-based Analysis of Language Lateralization and Cortical Asymmetry. *J. Cogn. Neurosci.* **25**, 1477–1492 (2013).
71. Winkler, A. M. *et al.* Measuring and comparing brain cortical surface area and other areal quantities. *Neuroimage* **61**, 1428–1443 (2012).
72. Bernal-Rusiel, J. L., Reuter, M., Greve, D. N., Fischl, B. & Sabuncu, M. R. Spatiotemporal linear mixed effects modeling for the mass-univariate analysis of longitudinal neuroimage data. *Neuroimage* **81**, 358–370 (2013).
73. Sørensen, Ø., Walhovd, K. B. & Fjell, A. M. A Recipe for Accurate Estimation of Lifespan Brain Trajectories, Distinguishing Longitudinal and Cohort Effects. (2020).
74. Wood, S. & Scheipl, F. gamm4: Generalized Additive Mixed Models using 'mgcv' and 'lme4'. R package version 0.2-5, available at https://cran.r-project.org/web/packages/gamm4/gamm4.pdf. (2017).
75. Dray, S. & Dufour, A. B. The ade4 package: Implementing the duality diagram for ecologists. *J. Stat. Softw.* **22**, 1–20 (2007).
76. Margulies, D. S., Falkiewicz, M. & Huntenburg, J. M. A cortical surface-based geodesic distance package for Python. *Gigascience* **5**, 1–26 (2016).
77. Schaefer, A. *et al.* Local-Global Parcellation of the Human Cerebral Cortex from Intrinsic Functional Connectivity MRI. *Cereb. Cortex* 1–20 (2017). doi:10.1093/cercor/bhx179
78. Neale, M. C. *et al.* OpenMx 2.0: Extended Structural Equation and Statistical Modeling. *Psychometrika* **81**, 535–549 (2016).
79. Jonsson, H. *et al.* Differences between germline genomes of monozygotic twins. *Nat. Genet.* **53**, 27–34 (2021).
80. Mayhew, A. J. & Meyre, D. Assessing the Heritability of Complex Traits in Humans: Methodological Challenges and Opportunities. *Curr. Genomics* **18**, 332–340 (2017).
81. Dalmaijer, E. S. Twin studies with unmet assumptions are biased towards genetic heritability. *bioRxiv* 2020.08.27.270801 (2020).
82. Bycroft, C. *et al.* The UK Biobank resource with deep phenotyping and genomic data. *Nature* **562**, 203–209 (2018).
83. Yang, J. *et al.* Common SNPs explain a large proportion of the heritability for human height. *Nat. Genet.* **42**, 565–569 (2010).
84. Fawns-Ritchie, C. & Deary, I. J. Reliability and validity of the UK Biobank cognitive tests. *PLoS One* **15**, 1–24 (2020).
85. Josse, J. & Husson, F. missMDA: A package for handling missing values in multivariate data analysis. *J. Stat. Softw.* **70**, (2016).
86. Xiang, L., Crow, T. J., Hopkins, W. D. & Roberts, N. Comparison of Surface Area and Cortical Thickness Asymmetry in the Human and Chimpanzee Brain. *Cereb. Cortex* 1–15 (2020). doi:10.1093/cercor/bhaa202
87. Long, X., Zhang, L., Liao, W., Jiang, C. & Qiu, B. Distinct laterality alterations distinguish mild cognitive impairment and Alzheimer's disease from healthy aging: Statistical parametric mapping with high resolution MRI. *Hum. Brain Mapp.* **34**, 3400–3410 (2013).
88. Habas, P. A. *et al.* Early folding patterns and asymmetries of the normal human brain detected from in utero MRI. *Cereb. Cortex* **22**, 13–25 (2012).
89. Glasel, H. *et al.* A robust cerebral asymmetry in the infant brain: The rightward superior temporal sulcus. *Neuroimage* **58**, 716–723 (2011).
90. Leroy, F. *et al.* New human-specific brain landmark: the depth asymmetry of superior temporal sulcus. *Proc. Natl. Acad. Sci. U. S. A.* **112**, 1208–13 (2015).
91. Geschwind, N. & Levitsky, W. Human Brain : Left-Right Asymmetries in Temporal Speech Region Published by : American Association for the Advancement of Science Stable URL : http://www.jstor.org/stable/1723941 Human Brain : Left-Right Asymmetries in Temporal Speech Region. **161**, 186–187 (1968).
92. Foundas, A. L., Eure, K. F., Luevano, L. F. & Weinberger, D. R. MRI asymmetries of Broca's area: The pars triangularis and pars opercularis. *Brain Lang.* **64**, 282–296 (1998).
93. Penfield, W. & Boldrey, E. Somatic Motor and Sensory Representation in Man. *Brain* 389–443 (1937).
94. Roux, F. E., Djidjeli, I. & Durand, J. B. Functional architecture of the somatosensory homunculus detected by electrostimulation. *J. Physiol.* **596**, 941–956 (2018).
95. Rumeau, C. *et al.* Location of hand function in the sensorimotor cortex: MR and functional correlation. *Am. J. Neuroradiol.* **15**, 567–572 (1994).
96. Walhovd, K. B. *et al.* Neurodevelopmental origins of lifespan changes in brain and cognition. *Proc. Natl. Acad. Sci. U. S. A.* **113**, 9357–9362 (2016).
97. Grasby, K. L. *et al.* The genetic architecture of the human cerebral cortex. *Science (80-.).* **367**, (2020).
98. Fjell, A. M. *et al.* Continuity and Discontinuity in Human Cortical Development and Change From Embryonic Stages to Old Age. *Cereb. Cortex* **29**, 3879–3890 (2019).
99. Wierenga, L. M., Langen, M., Oranje, B. & Durston, S. Unique developmental trajectories of cortical thickness and surface area. *Neuroimage* **87**, 120–126 (2014).
100. Brown, T. T. *et al.* Neuroanatomical assessment of biological maturity. *Curr. Biol.* **22**, 1693–1698 (2012).
101. Chance, S. A. The cortical microstructural basis of lateralized cognition: a review. *Front. Psychol.* **5**, 1–8 (2014).
102. Chance, S. A., Casanova, M. F., Switala, A. E. & Crow, T. J. Auditory cortex asymmetry, altered minicolumn spacing and absence of ageing effects in schizophrenia. *Brain* **131**, 3178–3192 (2008).
103. Tzourio-Mazoyer, N., Crivello, F. & Mazoyer, B. Is the planum temporale surface area a marker of hemispheric or regional language lateralization? *Brain Struct. Funct.* **223**, 1217–1228 (2018).
104. Ocklenburg, S. *et al.* Neurite architecture of the planum temporale predicts neurophysiological processing of auditory speech. *Sci. Adv.* **4**, 1–9 (2018).
105. Natu, V. S. *et al.* Apparent thinning of human visual cortex during childhood is associated with myelination. *Proc. Natl. Acad. Sci.* **116**, 20750–20759 (2019).
106. Petanjek, Z. *et al.* Extraordinary neoteny of synaptic spines in the human prefrontal cortex. *Proc. Natl. Acad. Sci. U. S. A.* **108**, 13281–13286 (2011).
107. Cizeron, M. *et al.* A brainwide atlas of synapses across the mouse life span. *Science (80-.).* **369**, 270–275 (2020).
108. Faust, T. E., Gunner, G. & Schafer, D. P. Mechanisms governing activity-dependent synaptic pruning in the developing mammalian CNS. *Nat. Rev. Neurosci.* **22**, 657–673 (2021).

109. Francks, C. Exploring human brain lateralization with molecular genetics and genomics. 1–13 (2015). doi:10.1111/nyas.12770
110. Cuellar-Partida, G. *et al.* Genome-wide association study identifies 48 common genetic variants associated with handedness. *Nat. Hum. Behav.* (2020). doi:10.1038/s41562-020-00956-y
111. Dubois, J. *et al.* Structural asymmetries of perisylvian regions in the preterm newborn. *Neuroimage* **52**, 32–42 (2010).
112. Kasprian, G. *et al.* The prenatal origin of hemispheric asymmetry: An in utero neuroimaging study. *Cereb. Cortex* **21**, 1076–1083 (2011).
113. Hill, J. *et al.* A Surface-Based Analysis of Hemispheric Asymmetries and Folding of Cerebral Cortex in Term-Born Human Infants. *J. Neurosci.* **30**, 2268–2276 (2010).
114. Bishop, D. V. M. & Bates, T. C. Heritability of language laterality assessed by functional transcranial Doppler ultrasound: A twin study. *Wellcome Open Res.* **4**, 1–52 (2020).
115. Somers, M. *et al.* Linkage analysis in a Dutch population isolate shows no major gene for left-handedness or atypical language lateralization. *J. Neurosci.* **35**, 8730–8736 (2015).
116. Hadžiselimović, H. & Čuš, M. Appearance of the base of the brain in relation to the configuration of human skull. *Acta Anat* **63**, 289–299 (1966).
117. Kong, X.-Z. *et al.* Handedness and Other Variables Associated with Human Brain Asymmetrical Skew. *bioRxiv* 756395 (2019). doi:10.1101/756395
118. Karama, S. *et al.* Childhood cognitive ability accounts for associations between cognitive ability and brain cortical thickness in old age. *Mol. Psychiatry* **19**, 555–559 (2014).
119. Deary, I. J., Whiteman, M. C., Starr, J. M., Whalley, L. J. & Fox, H. C. The Impact of Childhood Intelligence on Later Life: Following Up the Scottish Mental Surveys of 1932 and 1947. *J. Pers. Soc. Psychol.* **86**, 130–147 (2004).
120. Hansen, N. L. *et al.* Subclinical cognitive decline in middle-age is associated with reduced task-induced deactivation of the brain's default mode network. *Hum. Brain Mapp.* **35**, 4488–4498 (2014).
121. Logue, M. W. *et al.* Use of an Alzheimer's disease polygenic risk score to identify mild cognitive impairment in adults in their 50s. *Mol. Psychiatry* **24**, 421–430 (2019).
122. Labache, L. *et al.* A SENtence Supramodal Areas AtlaS (SENSAAS) based on multiple task-induced activation mapping and graph analysis of intrinsic connectivity in 144 healthy right-handers. *Brain Struct. Funct.* **224**, 859–882 (2019).
123. Biduła, S. P. & Króliczak, G. Structural asymmetry of the insula is linked to the lateralization of gesture and language. *Eur. J. Neurosci.* **41**, 1438–1447 (2015).
124. Keller, S. S. *et al.* Can the language-dominant hemisphere be predicted by brain anatomy? *J. Cogn. Neurosci.* **23**, 2013–2029 (2011).
125. Gerrits, R., Verhelst, H., Dhollander, T., Xiang, L. & Vingerhoets, G. Structural perisylvian asymmetry in naturally occurring atypical language dominance. *Brain Struct. Funct.* (2021). doi:10.1007/s00429-021-02323-7
126. Mazoyer, B. *et al.* Gaussian mixture modeling of hemispheric lateralization for language in a large sample of healthy individuals balanced for handedness. *PLoS One* **9**, 9–14 (2014).
127. Knecht, S. *et al.* Handedness and hemispheric language dominance in healthy humans. *Brain* **123**, 2512–2518 (2000).
128. Westerhausen, R. *et al.* The association of macro- and microstructure of the corpus callosum and language lateralisation. *Brain Lang.* **97**, 80–90 (2006).
129. Carey, D. P. & Johnstone, L. T. Quantifying cerebral asymmetries for language in dextrals and adextrals with random-effects meta analysis. *Front. Psychol.* **5**, 1–23 (2014).
130. Hervé, P. Y., Zago, L., Petit, L., Mazoyer, B. & Tzourio-Mazoyer, N. Revisiting human hemispheric specialization with neuroimaging. *Trends Cogn. Sci.* **17**, 69 (2013).
131. Afif, A., Bouvier, R., Buenerd, A., Trouillas, J. & Mertens, P. Development of the human fetal insular cortex: Study of the gyration from 13 to 28 gestational weeks. *Brain Struct. Funct.* **212**, 335–346 (2007).
132. Kalani, M. Y. S., Kalani, M. A., Gwinn, R., Keogh, B. & Tse, V. C. K. Embryological development of the human insula and its implications for the spread and resection of insular gliomas. *Neurosurg. Focus* **27**, 1–4 (2009).
133. Saadon-Grosman, N., Loewenstein, Y. & Arzy, S. The 'creatures' of the human cortical somatosensory system. *Brain Commun.* **2**, 1–10 (2020).
134. McCarrey, A. C., An, Y., Kitner-Triolo, M. H., Ferrucci, L. & Resnick, S. M. Sex differences in cognitive trajectories in clinically normal older adults. *Psychol. Aging* **31**, 166–175 (2016).
135. Lester, A. W., Moffat, S. D., Wiener, J. M., Barnes, C. A. & Wolbers, T. The Aging Navigational System. *Neuron* **95**, 1019–1035 (2017).
136. Wainschtein, P., Jain, D., Zheng, Z., Anthropometry, T. & Group, W. Recovery of trait heritability from whole genome sequence data Visscher 2019.pdf. 1–23 (2021).
137. Yang, J., Zeng, J., Goddard, M. E., Wray, N. R. & Visscher, P. M. Concepts, estimation and interpretation of SNP-based heritability. *Nat. Genet.* **49**, 1304–1310 (2017).
138. Gerrits, R., Verhelst, H., Vingerhoets, G. & Vingerhoets, G. Mirrored brain organization: Statistical anomaly or reversal of hemispheric functional segregation bias? *Proc. Natl. Acad. Sci. U. S. A.* **117**, 14057–14065 (2020).
139. Ocklenburg, S., Hirnstein, M., Beste, C. & Güntürkün, O. Lateralization and cognitive systems. *Washington, DC APA, Guidel. Dev. Panel Treat. Posttraumatic Stress Disord. Adults.* **5**, (2014).